Atmospheric Environment 346 (2025) 121075

Contents lists available at ScienceDirect

Atmospheric Environment

journal homepage: www.elsevier.com/locate/atmosenv

Trends of PM_1 aerosol chemical composition, carbonaceous aerosol, and source over the last 10 years at Melpitz (Germany)

Samira Atabakhsh [a], Laurent Poulain [a], Alessandro Bigi [b], Martine Collaud Coen [c], Mira Pöhlker [a], Hartmut Herrmann [a,*]

[a] Leibniz Institute for Tropospheric Research, 04318, Leipzig, Germany
[b] Department of Engineering 'Enzo Ferrari', University of Modena and Reggio Emilia, 41125, Modena, Italy
[c] Federal Office of Meteorology and Climatology, MeteoSwiss, 1530, Payerne, Switzerland

HIGHLIGHTS

- 10 years of annual and seasonal variability of PM_1 composition and sources at Melpitz.
- Analysis of air mass inflow direction on PM_1 components and their source contribution.
- Identification of decreasing PM_1 concentrations and 5 primary OA factors over a decade.
- Discussion of implications for air quality policies.

ARTICLE INFO

Keywords:
Long-range transport
Particulate matter (PM)
Trend analysis
Source apportionment
ACSM
Air quality
Organic aerosol

ABSTRACT

Submicron particles (PM_1) play a critical role in air quality, climate, and human health. Long-term monitoring is essential to identify changes in atmospheric composition driven by natural or anthropogenic emissions and processes. This study presents ten years of continuous measurements (Sept. 2012–Aug. 2022) at the TROPOS Melpitz research station in Germany, a Central European rural background site influenced by its location between Eastern and Western Europe. Using an aerosol chemical speciation monitor (ACSM) and a multi-angle absorption photometer (MAAP), alongside a rolling positive matrix factorization (PMF) model for organic aerosol (OA) source apportionment, we analyzed PM_1 trends, chemical composition, and source contributions over a decade. The results reveal a significant negative PM_1 trend of $-4.59\%\ y^{-1}$, with pronounced decreases occurring in fall and winter. Eastern air masses showed marked improvements ($-28\%\ y^{-1}$), likely reflecting regional mitigation policies. OA, contributing 44% of total PM_1, showed a negative trend of $-2.05\%\ y^{-1}$ and comprised three primary OA (POA) sources—hydrocarbon-like OA (HOA), biomass burning OA (BBOA), and coal combustion OA (CCOA)—and two oxygenated OA (OOA) factors (less-oxidized and more-oxidized OA, LO-OOA and MO-OOA). HOA (7% of total OA) remained relatively stable, with a minor decline ($-0.25\%\ y^{-1}$) under Eastern air masses. In contrast, BBOA (10% of OA) and CCOA (12% of OA) displayed strong seasonality, driven by residential heating and energy production. Notably, BBOA increased by $+0.48\ \%\ y^{-1}$ during summer, likely due to the rise in wood pellet heating, recreative, and/or wildfires, while CCOA showed a modest increase ($+0.27\%\ y^{-1}$) in Western air masses. The OOA factors, LO-OOA and MO-OOA (31% and 40% of OA, respectively), reflected distinct seasonal patterns tied to atmospheric formation pathways. Both showed declining trends in Eastern air masses ($-1.52\%\ y^{-1}$ and $-1.09\%\ y^{-1}$), indicating changes in biogenic emissions and/or anthropogenic precursors. Finally, eBC(PM_1) decreased by $-1.3\ \%\ y^{-1}$ with strong source dependency. Compared to urban areas, the overall decrease of PM mass concentration and anthropogenic OA looks limited, emphasizing a potentially lower effect of political mitigation outside cities. Overall, the findings underscore the importance of monitoring long-term changes in PM_1 composition and sources, which are crucial for understanding aerosol physical properties, refining climate models and public health, and evaluating the impacts of mitigation efforts on air quality and climate in different environments. Further studies on a similar approach are

* Corresponding author.
E-mail address: herrmann@tropos.de (H. Herrmann).

https://doi.org/10.1016/j.atmosenv.2025.121075
Received 6 September 2024; Received in revised form 21 December 2024; Accepted 25 January 2025
Available online 30 January 2025

strongly needed to better understand the geographical variation of the aerosol chemical composition and evaluate their potential effect.

1. Introduction

Atmospheric aerosol particles are characterized by their mass as particulate matter (PM in different size classes) and constitute a significant climate-forcing factor (IPCC, 2021) that also affects air quality and, hence, ecosystems and human health (Fowler et al., 2009; WHO, 2019). The PM chemical composition also shows a wide variety that arises from various natural or anthropogenic emissions, geographical locations, chemical processes, meteorological parameters, and different responses to atmospheric dynamics. According to air pollution reports from European countries, 293,000 deaths in 2021 were attributed to exposure to fine PM concentration above WHO's guideline level of 5 μg m^{-3} of air (European environment Agency, 2023). Accordingly, long-term measurements and trend analysis are needed to identify atmospheric aerosols and/or PM changes. Several studies have previously conducted long-term off-line filter measurements and trend analyses on different PM size ranges and various physical and chemical components of PM (e.g., Collaud Coen et al., 2020a; Cusack et al., 2012; Spindler et al., 2013). However, most of these cited studies depicted the change in the chemical compositions and did not relate to the behavior of the aerosol sources. There is a lack of knowledge about how aerosol particle sources, including both anthropogenic and biogenic, change over time and how this impacts the PM composition in a Central European target region. Of course, such a relation between observed particle composition and the causing contributions will and should affect air quality policies.

Among all the PMs, submicron PM, known as PM_1 (particles with an aerodynamic diameter of less than 1 μm), can travel hundreds of kilometers from their sources over days. Given that organic aerosol (OA) is the most abundant component of PM_1 (Jimenez et al., 2009), recognizing its sources remains a significant challenge. A way to access the OA source is to use online approaches based on, e.g., an aerosol mass spectrometer (AMS; Jayne et al., 2000) and an aerosol chemical speciation monitor (ACSM; Ng et al., 2011), which have been developed to provide mass spectral data for the non-refractory PM_1 (NR-PM_1) fraction. Subsequently, OA measured by AMS and ACSM can be further subdivided into different sources using receptor model approaches, particularly positive matrix factorization (PMF; Ulbrich et al., 2009; Canonaco et al., 2021). This study utilizes a novel source apportionment technique called rolling PMF (Canonaco et al., 2021) to analyze temporal variations in factor profiles. The non-rolling PMF algorithm encounters two primary limitations when applied over extended time periods. First, the factor profiles remain static throughout the duration of the analysis (Paatero, 1999). Second, the presence of rotational ambiguity leads to non-unique solutions. To mitigate these challenges, a multilinear engine (ME-2; Paatero, 1999) has been incorporated into the PMF analysis. This enhancement facilitates the integration of prior knowledge to steer the model towards environmentally plausible outcomes (e.g., Canonaco et al., 2013; Crippa et al., 2014). Additionally, to address the temporal variability in factor profiles, a rolling approach has been proposed (Parworth et al., 2015; Canonaco et al., 2021). This methodology employs a smaller PMF window (i.e., 14 days) that is systematically slid across the entire dataset with a 1-day interval, thereby enabling the capture of temporal changes in source profiles. Despite the large amount of measurements done with such instruments, most of them were focused on intensive field campaigns, and there is still a strong need for trend analysis focusing on PM_1 chemicals and OA sources from online measurements.

Most studies reporting long-term OA source apportionment using ACSM and/or AMS measurements have predominantly focused on urban traffic and urban background sites, where emissions are highest. Notable examples include a four-year dataset by Chebaicheb et al. (2023), a six-year dataset by Zhang et al. (2019), and a two-year dataset by Sun et al. (2018). However, rural sites are of great interest as they can represent the regional atmospheric background and the potential influence of long-range transport (LRT) of pollutants. Furthermore, multiyear investigations at rural and rural background sites are crucial for identifying long-term trends and understanding the impact of recent changes in emission sources. Indeed, one of the biggest limitations of the trend analysis is to properly consider the influence of individual months, meteorological seasons, and the cumulative impact of the predominant importance of the first and last year play an important role (Collaud Coen et al., 2020b). Therefore, to ensure robust trend results characterized by a lower confidence level (CL) and smaller slope, adhering to the standard recommendation of computing long-term trends over a time series spanning at least ten years is essential.

In this study, a 3 pre-whitening (3 PW) method (Collaud Coen et al., 2020b) has been applied not only to a decade-long dataset (total of 40 seasons) detailing PM_1 chemical composition but also to OA sources to detect their long-term trends in the monitoring site. Compared with alternative trend analysis methods, the 3 PW method demonstrates superior efficacy in maximizing statistical power. This approach significantly reduces the incidence of false trend identifications when no genuine trend exists. It delivers the most accurate slope estimates for the designated length of the time series (Collaud Coen et al., 2020b). Furthermore, since Melpitz is under the influence of either Eastern or Western air masses, representing Eastern and Western Europe, respectively (Spindler et al., 2010), a particular focus on the variation of PM is needed. However, studies of the effects of air mass inflow on PM for Melpitz station were, until now, either limited to a short period (one year in Atabakhsh et al., 2023) or a limited chemical composition description (OC/EC and water-soluble ions in Spindler et al., 2010, 2012, 2013) and they have limited the identification of source dependency.

Consequently, a comprehensive analysis of long-term PM_1 measurements at the Melpitz station, a rural background site situated between two distinct air masses from the east and west, is aimed for in this research. Through this study, the understanding of long-term trends in aerosol composition and mass concentrations is enhanced by identifying and analyzing the contributions of various sources and atmospheric processes. Seasonal and spatial variations in aerosol properties are explored, and trends in PM_1 chemical compositions and OA sources are examined. Additionally, practical insights are generated to support improvements in air quality management strategies, guide future emission reduction policies, and refine climate models by incorporating trends in the physical and chemical properties of aerosols.

2. Methodology

2.1. Measuring site

The long-term submicron aerosol measurements in this study were conducted at the TROPOS research station Melpitz (51.5255 N, 12.9277 E, 86 m a.s.l.) in a rural area around 50 km northeast of Leipzig, Germany (Birmili and Wiedensohler, 2000). The station has been monitoring the repercussions of long-range atmospheric transport on Central European background air quality since 1992 (Spindler et al., 2012). It is a Level 3 station within the European Monitoring and Evaluation Programme (EMEP) and integral to the Aerosol, Clouds, and Trace Gases Research Infrastructure (ACTRIS). The prevailing wind direction at Melpitz originates from the Southwest, characterized by maritime air masses, with intermittent influences from the city of Leipzig. In the winter season, the station experiences a significant influx of air from the

East, predominantly comprising dry continental air masses impacted by long-range transport of anthropogenic emissions (Spindler et al., 2010).

2.2. Instrumentation

2.2.1. Online instruments

This study measured NR-PM_1 (organic, sulfate, nitrate, ammonium, and chloride) using an Aerodyne quadrupole ACSM with a 30-min time resolution from September 2012 to the end of August 2022. The measurements were performed continuously, with a resulting data coverage of 76 % (details on data coverage in Fig. S1). The missing data is primarily attributed to participation in various inter-comparison workshops organized by the Aerosol Chemical Monitoring Calibration Center (ACMCC) near Paris, France, within the ACTRIS assurance/quality control (QA/QC) activities framework (fall 2014, 2016, and 2021). Technical malfunctions and maintenance periods also contributed to data gaps (critical period here as an example: fall 2015, winter 2017–2018, winter and spring 2019, spring and summer 2022). It resulted in three seasons with data coverage below 50 %. These seasons will still be considered but tagged with a small star sign. The ACSM sampling technique and operational procedures were previously described by Ng et al. (2011). Essentially, aerosols are focused into a narrow beam using an aerodynamic lens after (Liu et al., 2007) passage through a 100 μm orifice. Subsequently, NR-PM_1 material is evaporated at approximately 600 °C and ionized via electro-impact ionization at 70 eV before detection by a quadrupole mass spectrometer (RGA, Pfeiffer Vacuum Prisma Plus) every 30 s. The ACSM alternates between ambient and particle-free air measurements, allowing for generating aerosol mass spectra based on the difference between these two measurements. Signal spectra are converted into organic or inorganic species concentrations using a fragmentation table (Allan et al., 2004), ion transmission correction, and response factor (RF). Data processing adhered to the manufacturer's recommendations and ACTRIS requirements. Composition-dependent collection efficiency (CDCE) correction was applied based on the algorithms proposed by Middlebrook et al., (2012) to mitigate particle loss during vaporization. Further details regarding QA/QC procedures and instrumental uncertainties can be found in Poulain et al. (2020).

The eBC mass concentration was measured by a multi-angle absorption photometer (MAAP; model 5012 Thermo Scientific; Petzold and Schönlinner, 2004) within the PM_{10} range. The eBC mass concentration derived from the PM_{10} data was multiplied by a constant factor of 0.9, following the methodology of Poulain et al. (2011), to estimate the eBC mass concentration in the PM_1 fraction. As a result, all reported and discussed eBC mass concentrations here pertain to the eBC in the PM_1 fraction and are referred to as eBC(PM_1). Alongside the MAAP, a dual mobility particle size spectrometer (TROPOS-type T-MPSS; Birmili et al., 1999) was used to measure the particle number size distribution (PNSD) from 3 to 800 nm (mobility diameter, d mob) at both ambient and 300 °C temperatures (Wehner et al., 2002). The inlet for all online aerosol instruments, including the SMPS, ACSM, and MAAP, features a PM_{10} Anderson impactor located 6 m above ground level. This is followed by an automatic aerosol diffusion dryer, which actively maintains the relative humidity in the sampling line below 40% (Tuch et al., 2009). The flow is then split between the different instruments using an isokinetic splitter.

2.2.2. Offline instruments

Daily PM_{10} samples were collected using a high-volume sampler (DIGITEL DHA-80, Digitel Elektronik AG, Hegnau, Switzerland) equipped with a quartz filter for 24 h, from midnight to midnight. For detailed information regarding sample preparation and evaluation methods, refer to Spindler et al. (2013) or Poulain et al. (2020). Following Iinuma et al. (2009), levoglucosan was measured as a tracer for wood-burning combustion using high-performance anion exchange chromatography coupled with an electrochemical detector (HPAEC-PAD).

2.2.3. Gas monitoring and meteorological parameters

As previously described by Ren et al. (2020), NO and NO_2 levels were assessed using a customized Trace Level NO_x Analysis Model 42i-TL (Thermo Scientific) equipped with a blue light converter. Additionally, routine measurements encompassed temperature, relative humidity, solar radiation, precipitation, wind direction, and wind speed.

2.3. Spatial classification of PM_1

Determining air mass origin followed the methodology established by Spindler et al. (2010),which integrates wind direction with air mass backward trajectories. Backward trajectories spanning 96 h were computed twice daily (at 10:00 and 18:00 Central European time) at 200, 500, and 1500 m above ground level using the NOAA Hybrid single-particle lagrangian integrated trajectory (Hysplit) Model (source: http://www.arl.noaa.gov/ready/hysplit4.htm; Draxler and Rolph, 2014). The classification of air masses into Eastern and Western sectors was based on wind direction criteria, with the Eastern sector encompassing air mass transport from the East (wind direction ranging from 35° to 140°) and the Western sector corresponding to air masses originating from the West (wind direction ranging from 210° to 320°). Days characterized by local influences, significant directional shifts, or winds from the North (320°–35°) or South (140°–210°) were excluded from the averages for the Western and Eastern air mass classifications. It is important to note that this method's separation of days involves subjective judgment. For comprehensive details, refer to Spindler et al. (2010).

The study's findings are categorized based on the time of the year and air masses. Regarding timing splitting, the entire measurement period will be later called "decade". At the same time, the different meteorological seasons are "fall" (September, October, November), "winter" (December, January, February), "spring" (March, April, May), and "summer" (June, July, August). For air masses, the data will be available for the entire dataset as "entire", for the Western air mass as "Western," and for the Eastern air mass as "Eastern". For instance, the "decade Western" corresponds to all the measurement periods associated with Western air masses and "fall entire" to all the measurements performed during fall without any air mass classification.

2.4. Trend analysis

The multi-year trends of the hourly mean dataset in this study were analyzed using the 3 PW algorithm introduced by Collaud Coen et al. (2020b), implemented in RStudio software (Bigi and Vogt, 2021). This 3 PW algorithm integrates the Mann-Kendall test and Theil-Sen slope estimator, aiming to mitigate both type 1 and type 2 errors (wherein type 1 error refers to an erroneous rejection of the null hypothesis, i.e., a false positive, and type 2 error denotes an erroneous acceptance of the null hypothesis, i.e., a false negative), along with challenges associated with slope modification resulting from the application of three distinct PW methods.

The conventional PW method, which eliminates the first lag autocorrelation (Kulkarni and Von Storch, 1995), is associated with a notably low type 1 error and low test power. Conversely, the trend-free PW procedure developed by Yue et al. (2002) (referred to as TFPW-Y in Collaud Coen et al., 2020b) restores test power, albeit at the expense of the type 1 error. Both these PW techniques were employed prior to the Mann-Kendall (MK) test to evaluate the statistical significance of the trend. A trend was deemed statistically significant only if both PW and TFPW-Y exhibited significance at the 95 % confidence level or if PW was statistically significant while TFPW-Y was not (resulting in a false negative). Following the determination of statistical significance, a third PW procedure, the variance-corrected trend-free PW procedure (VCTFPW), was applied to enhance slope accuracy (Wang et al., 2015) prior to Sen's slope estimation. The confidence limits for Sen's slope were computed at the 90 % confidence level. Given the clear seasonal

cycles in the investigated data, the modified seasonal MK test (Hirsch et al., 1982) was consistently applied across the four meteorological seasons.

2.5. Rolling PMF analysis

Detailed information on the rolling PMF data processing for the one-year dataset at Melpitz is available in Atabakhsh et al. (2023), following the standardized protocol and criteria suggested by Chen et al. (2022). The seasonal pre-test for the four meteorological seasons was conducted by Atabakhsh et al. (2023), helping to ensure that the POA factors were correctly constrained and that irrelevant sources were not forced to be resolved across different seasons. Then, in work by Atabakhsh et al. (2023) bootstrap analysis and rolling PMF were applied, and the constraints applied through ME-2 for hydrocarbon-like OA (HOA) and biomass burning OA (BBOA) sources used the anchor profile of Crippa et al. (2014) and Ng et al. (2011), respectively. The anchor profile used for coal combustion OA (CCOA) in work by Atabakhsh et al. (2023) was generated from their winter data over one year of data analysis. For each of the four seasons, primary profiles were subject to a sensitivity analysis with a-values ranging from 0 to 0.4 for HOA and BBOA and 0–0.5 for CCOA, and steps of 0.1 were used to choose the best a-value combination for these three factors by Atabakhsh et al. (2023). Based on Atabakhsh et al. (2023) work, yearly PMF analysis was performed for each of the years considered in this work to cover the entire decade by using the same reference mass spectra for the three primary OAs (POA; HOA, BBOA, and CCOA) as in Atabakhsh et al. (2023). The rolling parameters were set to a 14-day window, a 1-day shift, and 100 repeats per window for every ten PMF inputs.

Briefly, to perform the multi-year analysis of OA sources, the PMF method (Paatero, 1999) was used with Igor Pro software (version 8.04, Wavemetrics, Inc., Lake Oswego, OR, USA) and source finder professional (SoFi Pro, version 8.04, Canonaco et al., 2021). Constraints based on prior knowledge were applied to prevent the mixing of primary factors (Canonaco et al., 2013; Crippa et al., 2014). The multilinear engine (ME-2) algorithm (Paatero, 1999) was used to incorporate time series and factor profile constraints. In the PMF method, the dataset X is decomposed into factor profiles (F) and factor contributions (G), with the residual matrix (E) representing the dataset that the model cannot describe. The dimensions of F and G are determined by the number of factors selected to represent the user-defined data:

$$X_{ij} = \sum_{k=1}^{p} G_{ik} \times F_{kj} + E_{ij} \quad (1)$$

This analysis identified five factors at Melpitz: three POAs— HOA, BBOA, and CCOA—and two oxygenated OAs—low oxidized oxygenated OA (LO-OOA) and more oxidized oxygenated OA (MO-OOA).

2.6. eBC(PM_1) source apportionment

The eBC(PM_1) data from the MAAP measurements were further segregated into POA factors since a correlation between eBC(PM_1) and each of the POA factors can be found similarly than previously observed in the one-year analysis from Atabakhsh et al. (2023). Therefore, a multilinear regression model was used, as suggested by Laborde et al., (2013), Zhu et al., (2018), and Poulain et al. (2011). This method presupposes that eBC(PM_1) mass is associated with the separate contribution from each OA factor (i.e., $eBC(PM_{1HOA})$, $eBC(PM_{1BBOA})$, and $eBC(PM_{1CCOA})$) at any given time. As a simple equation, the model can be expressed as:

$$eBC(PM_1(t)) = eBC(PM_{1HOA}(t)) + eBC(PM_{1BBOA}(t)) + eBC(PM_{1CCOA}(t)) \quad (2)$$

Each source of eBC(PM_1) emission should be proportional to the separate source mass concentration generated in each season (m_{HOA}, m_{BBOA}, and m_{CCOA}, respectively). As a result, the multilinear regression model is as follows:

$$eBC(PM_1(t)) = am_{HOA} + bm_{BBOA} + cm_{CCOA} \quad (3)$$

where a, b, and c are the linear regression coefficients for m_{HOA}, m_{BBOA}, and m_{CCOA}, respectively, which will be used to assess the contribution of eBC(PM_1) to each POA factor for each season.

3. Results and discussion

3.1. Chemical composition and trend analysis of PM_1

Fig. 1 presents the time series and overall averaged mass concentration of PM_1 chemicals at Melpitz during the observation period.

The mean mass concentration of total PM_1 for the decade (entire measurement period) was 9.79 μg m^{-3}, with the highest mean mass concentration observed in winter and the lowest in summer (12.07 μg m^{-3} and 8.3 μg m^{-3}, respectively; Table S1). Comparing these results with previous AMS and ACSM measurements at Melpitz station, the total PM_1 showed a similar mean mass concentration in different periods and followed the same seasonal trend; Atabakhsh et al. (2023) reported a total PM_1 mean mass concentration of 10.49 μg m^{-3} from September 2016 to August 2017. Similarly, Poulain et al. (2020) found a mean mass concentration of 10.23 μg m^{-3} from 2012 to 2017. Both studies presented the highest mass concentration in winter and the lowest in summer; Atabakhsh et al. (2023) reported 15.95 μg m^{-3} for winter and 6.24 μg m^{-3} for summer, and Poulain et al. (2020) reported 13.15 μg m^{-3} for the winter and 7.64 μg m^{-3} for the summer season.

OA was the most abundant component, with an annual mean mass concentration of 4.35 μg m^{-3} and a mass contribution of 44 % to the total PM_1 (see Fig. 1, Table S1). This is followed by nitrate, sulfate, ammonium, and eBC(PM_1) with average mass concentrations of 2.3 μg m^{-3}, 1.53 μg m^{-3}, 1.12 μg m^{-3}, and 0.57 μg m^{-3}, respectively, and mass contribution of 24 %, 15 %, 11 %, and 6 % to the total PM_1. Chloride will not be considered further in this analysis due to its very low mass concentration and contribution (0.02 μg m^{-3} and less than 1 %, respectively) and limited detection, as described by Crenn et al., (2015). The OA contribution to total PM_1 in this study falls within the range observed at other European rural background sites (44 %–55 %, Chen et al., 2022). Among the inorganic PM_1 components, nitrate emerged as the most significant component, similar to other rural-background sites in Europe such as Kosetice, Magadino, Carnsore Point, Sitra, Cabauw, and Ispra (Bressi et al., 2021; Chen et al., 2022). Furthermore, Bressi et al. (2021) reported a higher contribution of nitrate at rural background sites in Central Europe than those in Northern or Southern Europe.

3.1.1. Temporal and seasonal variation of PM_1 chemical components

Fig. 2 displays the results of long-term sampling and characterization of PM_1 chemical composition with hourly resolution for different years and seasons. Fig. 3 illustrates the average concentration during different yearly periods based on air masses and meteorological seasons.

The yearly mean of total PM_1 mass concentration across different seasons ranged from 5.63 μg m^{-3} in the fall of 2019 to 15.98 μg m^{-3} in the winter of 2016-17 (see Fig. 2 and Table S3). Although the total PM_1 mass concentration during summer remained relatively constant from year-to-year, other seasons clearly showed more important year-to-year variations. The highest variability in mean concentration was observed during winter (Fig. 2), with values ranging from 6.87 μg m^{-3} in the year 2019-20 to 15.98 μg m^{-3} in the year 2016-17. Additionally, higher average winter concentrations were linked to lower mean temperatures for the corresponding year (Fig. S4). Furthermore, the seasonal variability of mass concentration of chemical components across different years (Fig. 2) can be primarily attributed to variations in emissions sources and meteorological conditions, which indirectly influence

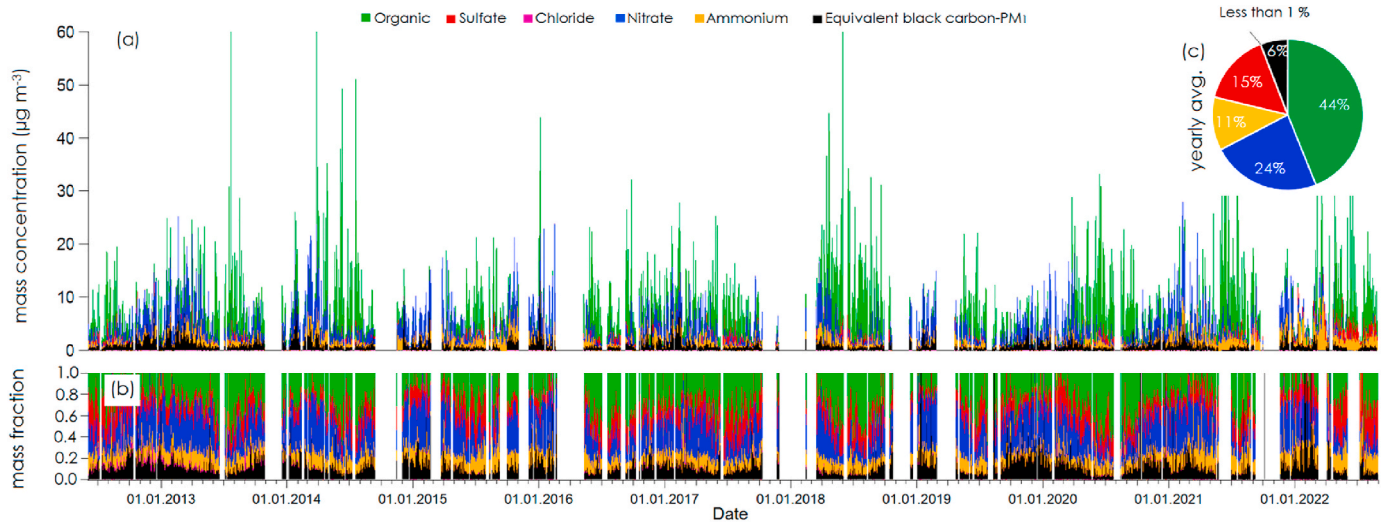

Fig. 1. Time series of (a) the particulate PM_1 chemical composition, (b) the corresponding mass contribution, and (c) the average contribution of each chemical component (time is in UTC).

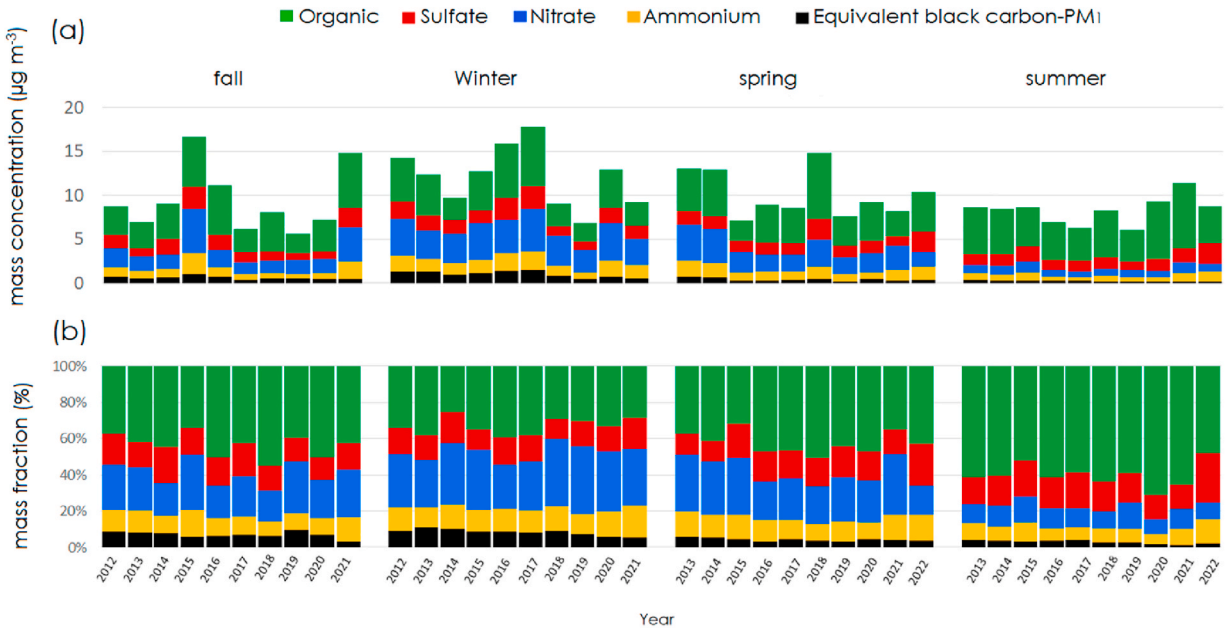

Fig. 2. (a) yearly mean mass concentration of the particulate PM_1 chemical composition, and (b) the corresponding mass contribution.

concentration through factors such as mixing layer height, temperature, and precipitation.

In terms of PM_1 chemical components and by looking at individual species, only nitrate emphasizes a particular variability among all inorganic compounds (Fig. 2). Elevated nitrate levels in spring were associated with heightened ammonia (NH_3) emissions from agricultural activities surrounding Melpitz station (Stieger et al., 2018)). In winter, higher nitrate levels could be linked to favorable photochemical and low-temperature conditions for forming ammonium nitrate (NH_4NO_3, Bressi et al., 2021). During summer, the mass concentration and contribution of nitrate and ammonium decreased due to the evaporation of ammonium nitrate. The highest contribution of nitrates was associated with the Western air mass (Fig. 3), reflecting the impact of NO_x sources from traffic and industry, as well as ammonia (NH_3) from agricultural activities in Central and Western Europe (Tichý et al., 2023; Velthof et al., 2012). Atabakhsh et al. (2023) also showed a higher contribution of nitrate in Western air masses for all seasons. In contrast, sulfate levels were fairly consistent regarding seasonal mass concentrations and contributions throughout the period. In addition, the mass contribution of sulfate remained stable across both Eastern and Western air masses (16 % for both air masses). eBC(PM_1) presented the highest mass concentration and contribution during the winter (1.03 µg m^{-3} or 9 % of total PM_1 vs. 0.24 µg m^{-3} or 4 % of total PM_1 in summer), primarily due to domestic heating activities and the reduced dilution associated with the dynamic of the mixing layer height. However, in the Eastern air mass, eBC(PM_1) exhibited a higher mass concentration of 1.15 µg m^{-3} compared to the Western air mass, which recorded 0.36 µg m^{-3}. This difference is attributed to anthropogenic emissions originating from Eastern source regions (Spindler et al., 2010).

Finally, OA, the most abundant component of PM_1, had various seasonal variability, with yearly mean values ranging from 2.0 µg m^{-3} (winter 2019-20) to 7.4 µg m^{-3} (summer 2021). OA showed the highest mass contribution during summer (61 %), attributed to a more critical secondary organic aerosol production. Like eBC(PM_1), OA displayed its

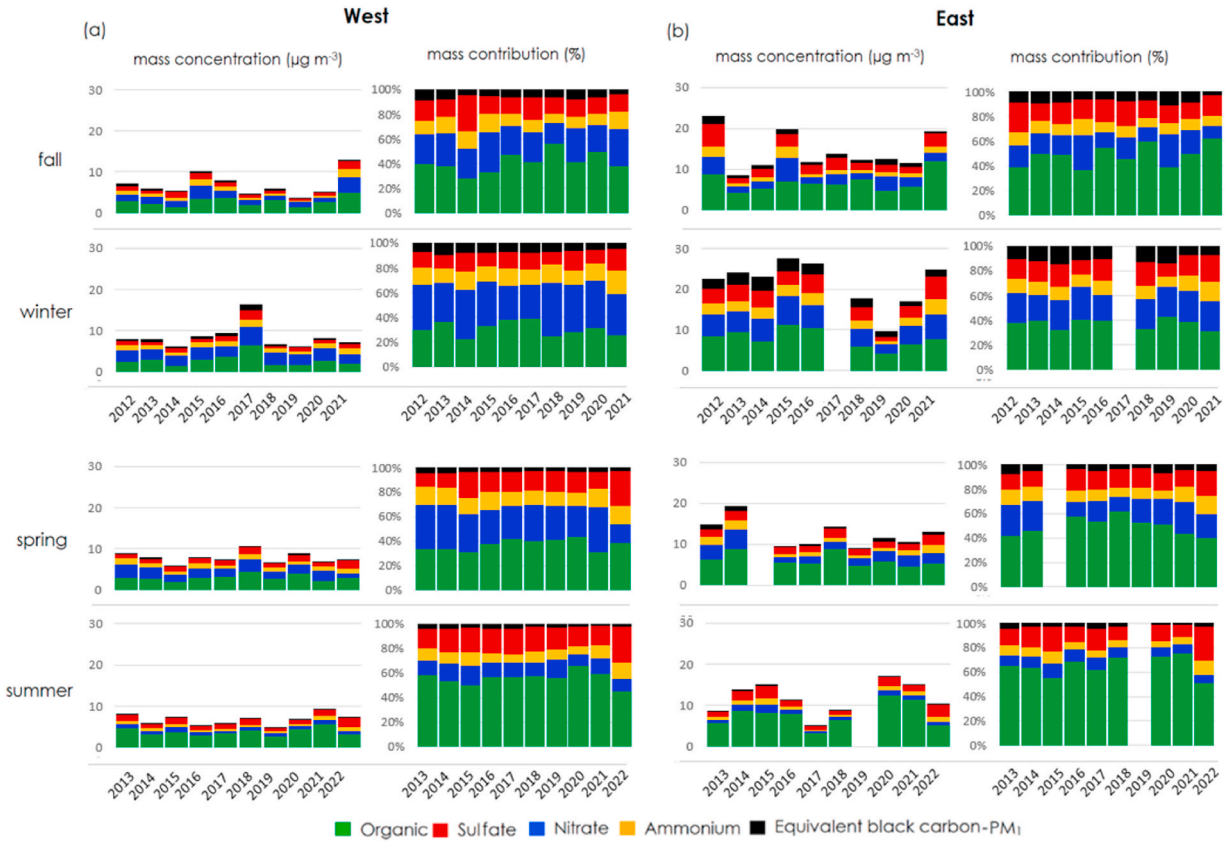

Fig. 3. Yearly mean mass concentration and mass contribution of the particulate PM_1 chemical composition for (a) Western air mass and (b) Eastern mass for different meteorological seasons.

highest contribution during periods of Eastern airmass influence (48 % vs. 41 % from Western airmass), likely due to anthropogenic activities in Eastern regions.

3.1.2. *Trend analysis of PM_1 chemical components*

Fig. 4 illustrates the trend results of the hourly resolution dataset of total PM_1 mass and chemical composition over a decade, categorized by seasons (fall, winter, spring, and summer), by the two main air mass sectors (Western and Eastern) and entire for the complete dataset without any air mass classification. The analysis of mass concentration and mass contribution provides complementary perspectives on aerosol trends, each influenced by distinct factors and analytical methods. Mass concentration measurements are heavily impacted by dilution, environmental mixing, temporal and spatial heterogeneity, and fluctuations in emission sources. These influences introduce substantial variability and dispersion in the data, often masking trends and leading to reduced statistical significance in slope analyses. In contrast, mass contribution data is more directly linked to the interactions among aerosol components, offering a clearer representation of compositional trends and often yielding more pronounced and interpretable results. However, a critical aspect of mass contribution analysis is that the total must sum to 100%, enabling trends for individual compounds to be assessed independently without enforcing equilibrium between increasing and decreasing trends. Moreover, in the examination of trend results, it is essential to focus exclusively on statistically significant trends. Non-significant trends should be disregarded, as they do not provide reliable insights into changes and may be indistinguishable from trends that indicate no change (Collaud Coen et al., 2020b).

3.1.2.1. PM_1 mass. The total PM_1 mass concentration exhibited a statistically significant negative trend of -0.04 µg m^{-3} y^{-1} (-4.59 % y^{-1}, Fig. 4a–Table S7) over the entire period in a decade. The PM_1 level measured at the Melpitz station was lower than expected compared to other rural stations across Germany in the $PM_{2.5}$ and PM_{10} ranges, showing a decrease of approximately ≈ -2.5 µg m^{-3} for both size ranges from 2012 to 2022 (Kessinger et al., 2024). This suggests that the initiatives to improve air quality did not adequately address these particular types of aerosols or cover the geographical areas from which the air masses originated. Regarding seasonal trends, a significant negative trend was only identified in fall and winter for the entire dataset (-0.11 µg m^{-3} y^{-1} and -0.12 µg m^{-3} y^{-1}, respectively), without significantly impacting the air mass classification at Melpitz station. All the other slopes were not statistically significant. Moreover, consistent with previous studies conducted at the Melpitz station (Atabakhsh et al., 2023; Spindler et al., 2010, 2013), air masses originating from Eastern Europe were generally more polluted than those from Western Europe, regardless of year-to-year variations (Fig. S3). To determine if the disparity between the two air masses is changing over time, the difference between the total PM_1 levels of Eastern and Western air masses (here known as *"DIFF"* $= mass\ concentration_{East} - mass\ concentration_{West}$) was also investigated (Fig. S3), and a significant decrease of -0.28 µg m^{-3} y^{-1} (-28 % y^{-1}) was found. This reduction can also be explained by the significant reduction of total PM_1 mass concentration for the Eastern air mass (-0.07 µg m^{-3} y^{-1} or -7.23 % y^{-1}) (Table S8), while the change in the Western air mass was not statistically significant. The reduction of DIFF emphasizes that over the past decade, Eastern Europe has seen a significant improvement in air quality, which can certainly be associated with the different local air quality policies.

The observed decreasing trend in PM_1 concentration at the Melpitz station is consistent with previous studies conducted at various locations across Europe. For instance, a decreasing trend in PM_{10} concentration was reported in a previous study for the Melpitz station spanning from 1993 to 2000 (Spindler et al., 2013)). Similarly, other long-term trend analyses of different PM size ranges at various European locations have

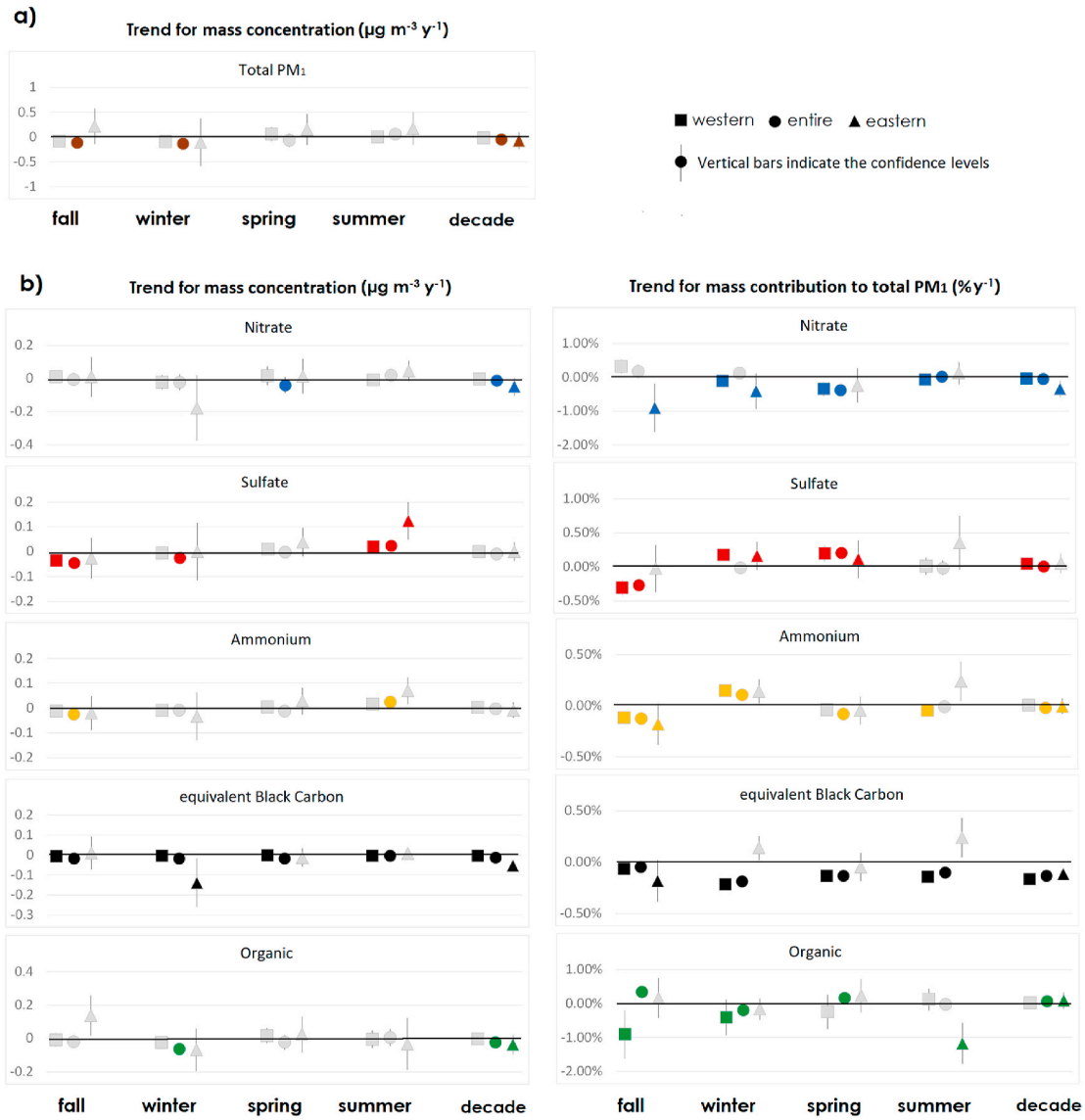

Fig. 4. Seasonal MK trend results for Melpitz station with long time series based on different seasons and the annual average for (a) total PM_1 mass concentration and (b) the mass concentration and mass contribution of chemical components. The colored is statistically significant, whereas grey is not a statistically significant trend. The slope of the Western trend is shown by the square (■), entire by the circle (●), and Eastern by triangle (▲), and vertical bars indicate the upper and lower confidence levels.

also shown decreasing trends. Chen et al. (2024) reported a decreasing trend in $PM_{2.5}$ (−1.72 % y^{-1}) and PM_{10} (−2.74 % y^{-1}) from 2003 to 2019 across 35 European countries. Another study by Zhang et al. (2019) reported a decrease in PM_1 concentration (−0.64 μg m^{-3} y^{-1}) over six years (2012–2018) at a peri-urban background station near Paris (SIRTA). This gradual reduction in PM concentration is likely attributed to implementing of mitigation strategies across European countries to reduce air pollution (European Parliament and Council of the European Union, 2008). The differences in trend slopes between the current and previous studies can be attributed to several factors. These include the impact of the mitigation policies across different types of monitoring stations (e.g., urban background vs. rural background stations), differences in the methods used to calculate trend slopes, and differences in the study periods and time resolutions employed. Additionally, it is important to note that trend slopes tend to have larger absolute values for shorter periods due to cumulative effects, particularly from the first and last years of the study period (Collaud Coen et al., 2020b).

3.1.2.2. Nitrate. Nitrate showed a significant trend with a slight reduction of −1.1 % y^{-1} (−0.01 μg m^{-3} y^{-1}, Fig. 4b), which can be principally linked to the decrease in nitrate mass concentration in Eastern air masses (−0.05 μg m^{-3} y^{-1}, -5 % y^{-1}). This trend aligns with PM_1 results from SIRTA (−0.14 μg m^{-3} y^{-1}, Zhang et al., 2019). Except for the small negative trend in spring, no significant seasonal change in the nitrate concentration nor further dependency on the air mass origin was found. This decreasing trend in nitrate concentration may be attributed solely to the NO_x emissions control in Europe, although the reduction of NH_3 was not as significant during this period (European Environment Agency, 2023). However, looking at the trend of the nitrate mass contributions to the total PM_1, a clearer trend emerged with a negative value of −0.05 % y^{-1} for the decade on entire data as well as for both Western and Eastern air masses (−0.03 % y^{-1} and -0.34 % y^{-1}, respectively). Interestingly, this trend was more pronounced in fall and winter periods for the Eastern air masses (−0.90 % y^{-1} and -0.41 % y^{-1}, respectively), while it happened during winter, spring, and summer for the Western ones (−0.11 % y^{-1}, -0.34 % y^{-1}, and -0.06 % y^{-1}; respectively). This result emphasizes that, even though no clear change in

nitrate mass concentration was found, the interactions between the different species led to a statistically significant decrease in the nitrate contribution to the total PM_1.

3.1.2.3. Sulfate. Although no significant trend in sulfate mass concentration was observed neither for the entire decade nor the overall two-air mass origins, significant seasonal trends were identified. Notably, a significant negative trend of sulfate mass concentration was observed during the fall (for both Western and entire sectors, -0.03 μg m^{-3} y^{-1} and -0.04 μg m^{-3} y^{-1}, respectively, representing a decrease of -3.6 % y^{-1} and -4.4 % y^{-1}) and winter (entire -0.02 μg m^{-3} y^{-1} or -2.4 % y^{-1}). The slope turned out to be significantly positive during summer for all three sectors (Western, entire, and Eastern; $+0.02$ μg m^{-3} y^{-1}, $+0.02$ μg m^{-3} y^{-1}, and $+0.12$ μg m^{-3} y^{-1}, or $+2.0$ % y^{-1}, $+2.5$ % y^{-1}, and $+12.4$ % y^{-1}, respectively). The increase in sulfate during summer could be explained by the frequency of new particle formation (NPF), as indicated by Bousiotis Pope et al. (2021), who demonstrated a higher growth rate in summer at rural background stations than in other seasons. Similar trends in sulfate concentration at the PM_1 range have been reported in other studies, such as a negative trend of -0.02 μg m^{-3} y^{-1} for SIRTA Zhang et al. (2019). Furthermore, the mass contribution trend of sulfate presented a significant negative trend only during fall (for both the Western sector and the entire data), while it shows a positive trend for the rest of the seasons for all three regimes: Eastern, Western, and entire (Fig. 4b). This underscores the critical role of NPF at this research station, particularly in terms of inorganic components, where sulfate plays a significant role in particle formation and composition.

3.1.2.4. Ammonium. Ammonium can exist in forms such as ammonium-nitrate and ammonium-sulfate; however, its mass concentration did not show a significant trend over the decade resolution. However, significant slopes were observed in fall, showing a decrease of -0.02 μg m^{-3} y^{-1} or -2.3 % y^{-1}, and in summer, indicating an increase of $+0.02$ μg m^{-3} y^{-1} by $+2.5$ % y^{-1}. In terms of mass contribution, ammonium presented a significantly decreasing trend over the decade resolution (for the entire dataset) and more especially during falls (for all three regimes) and spring (for the entire dataset) seasons (Fig. 4b). The trend slopes were significant over the decade resolution for Western airmass and on a seasonal basis during winter and summer for both Western and entire regimes (Fig. 4b).

3.1.2.5. Black carbon. The concentration trends of $eBC(PM_1)$ exhibited a notable negative trend across most seasons and air mass regimes, e.g., for the entire dataset over the decade, was -1.3 % y^{-1} (-0.012 μg m^{-3} y^{-1}). However, the trends in fall, spring, and summer for the Eastern air mass did not demonstrate statistical significance, as illustrated in Fig. 4b. A previous study for the Melpitz station conducted by Sun et al. (2020) for PM_{10} range also reported a negative trend with a decrease of -4.4 % y^{-1} for eBC concentration from 2009 to 2018. The differences observed in the trend slopes of Melpitz eBC in the present study and the work by Sun et al. (2020) can be attributed to variations not only in calculation methods, study periods, and time resolutions but also to the impact of emission mitigation policies implemented during the respective study periods. Similar trends of decreasing eBC and/or EC have been observed across different European locations and PM ranges, such as those reported by Zhang et al. (2019), and Spindler et al. (2013). eBC and/or EC are primarily emitted from combustion processes, including fossil fuel combustion in vehicles, industrial activities, and residential heating. Like mass concentration trends, $eBC(PM_1)$ contribution exhibited statistically significant negative trends for most seasons and regimes (e.g., entire decade -0.13 % y^{-1}); an exception is the Eastern air mass $eBC(PM_1)$, which was only significant for falls (-0.20 % y^{-1}; Fig. 4b). This suggested that while overall reductions in $eBC(PM_1)$ were evident, the seasonal and regional variations highlighted the complexities in emission sources and atmospheric processes affecting $eBC(PM_1)$ concentrations. The observed decrease in $eBC(PM_1)$ can be attributed to implementing emission control measures, such as the transition towards cleaner fuels, increased gas and renewable energy use, and improvements in combustion technologies. To better understand the change over the last decade in $eBC(PM_1)$ concentration, it is therefore critical to identify the different sources of $eBC(PM_1)$. A detailed discussion of combustion and burning-related $eBC(PM_1)$ trends will be presented in Section 3.2.

3.1.2.6. Organics (OA). Finally, the averaged OA concentration over a decade showed a significant decreasing trend of -0.02 μg m^{-3} y^{-1} (corresponding to -2.05 % y^{-1}) for the entire period in a decade, which was undoubtedly driven by the negative trend of winter (-0.06 μg m^{-3} y^{-1}, -6.17 % y^{-1}), the only significant one. When considering air mass classification, only the Eastern air mass showed a significant decadal trend in OA concentration, decreasing by -0.03 μg m^{-3} y^{-1} (-3.46 % y^{-1}). This trend aligns with findings from another study, which reported a negative OA concentration trend in the PM_1 range (-0.38 μg m^{-3} y^{-1} at the SIRTA station, Zhang et al. (2019). However, the OA contribution to total PM_1 showed a different behavior depending on the season. On a decadal scale, there was a slight positive trend in OA contribution for the entire data set, and Eastern air mass was considered (entire and Eastern, $+0.08$ % y^{-1} and $+0.09$ % y^{-1}, respectively). The OA contribution to PM_1 showed an increasing trend in both fall and spring, while a negative trend was observed for winter. Changes in OA concentration over time can reflect changes in emissions as well as in atmospheric processes. Consequently, it is necessary to investigate the change in the OA sources, which will help clarify the factors influencing OA concentrations and contributions, shedding light on the complex interplay between emissions, atmospheric processes, and seasonal variations in a similar way to eBC. To better understand these varying trends, the next section (Sec. 3.3.2) will delve into the different OA sources and their trends across different seasons and air masses.

3.2. Overview and trend analysis of OA PMF sources

The mean mass concentration and contribution of OA sources, along with their factor profiles, are illustrated in Fig. 5. Extending the approach developed by Atabakhsh et al. (2023) from a one-year study at Melpitz to ten years, which allowed for identifying the same five OA factors. Comprehensive details on these factors are available in the mentioned study of Atabakhsh et al. (2023) and are briefly summarized here. Hydrocarbon-like OA (HOA) had the lowest mean mass concentration at 0.3 μg m^{-3} (7 % of total OA), characterized by specific peaks at *m/z* 41, 43, 55, and 57, associated with alkyl and alkenyl fragments. Biomass burning OA (BBOA), with a mean mass concentration of 0.43 μg m^{-3} (10 % of total OA), was distinguished by the significant presence of ions at *m/z* 60 and 73, commonly linked to biomass burning. Coal combustion OA (CCOA), with a mean mass concentration of 0.52 μg m^{-3} (12 % of total OA), featured fragments at *m/z* 77, 91, and 115, related to polycyclic aromatic hydrocarbons (PAHs). Results from the multilinear regression model between $eBC(PM_1)$ and primary OA factors (HOA, BBOA, and CCOA; Fig. S6) indicated that BBOA and CCOA contributed significantly to $eBC(PM_1)$, accounting for 51 % and 47 % of POA, respectively.

More oxidized oxygenated OA (MO-OOA) had a mean mass concentration of 1.73 μg m^{-3} (40 % of total OA) and was characterized by a strong peak at *m/z* 44, indicating a higher oxidation state. Low oxidized oxygenated OA (LO-OOA), with a mean mass concentration of 1.35 μg m^{-3} (31 % of total OA), showed variability at *m/z* 43 and 44 and was influenced by other ions such as *m/z* 29 and 55, consistent with spectra from other studies (Atabakhsh et al., 2023; Chen et al., 2021; Tobler et al., 2021). From the mass contribution time series (Fig. 5b), MO-OOA emerged as the dominant factor over the entire period, suggesting its strong association with aging and photochemical processes across

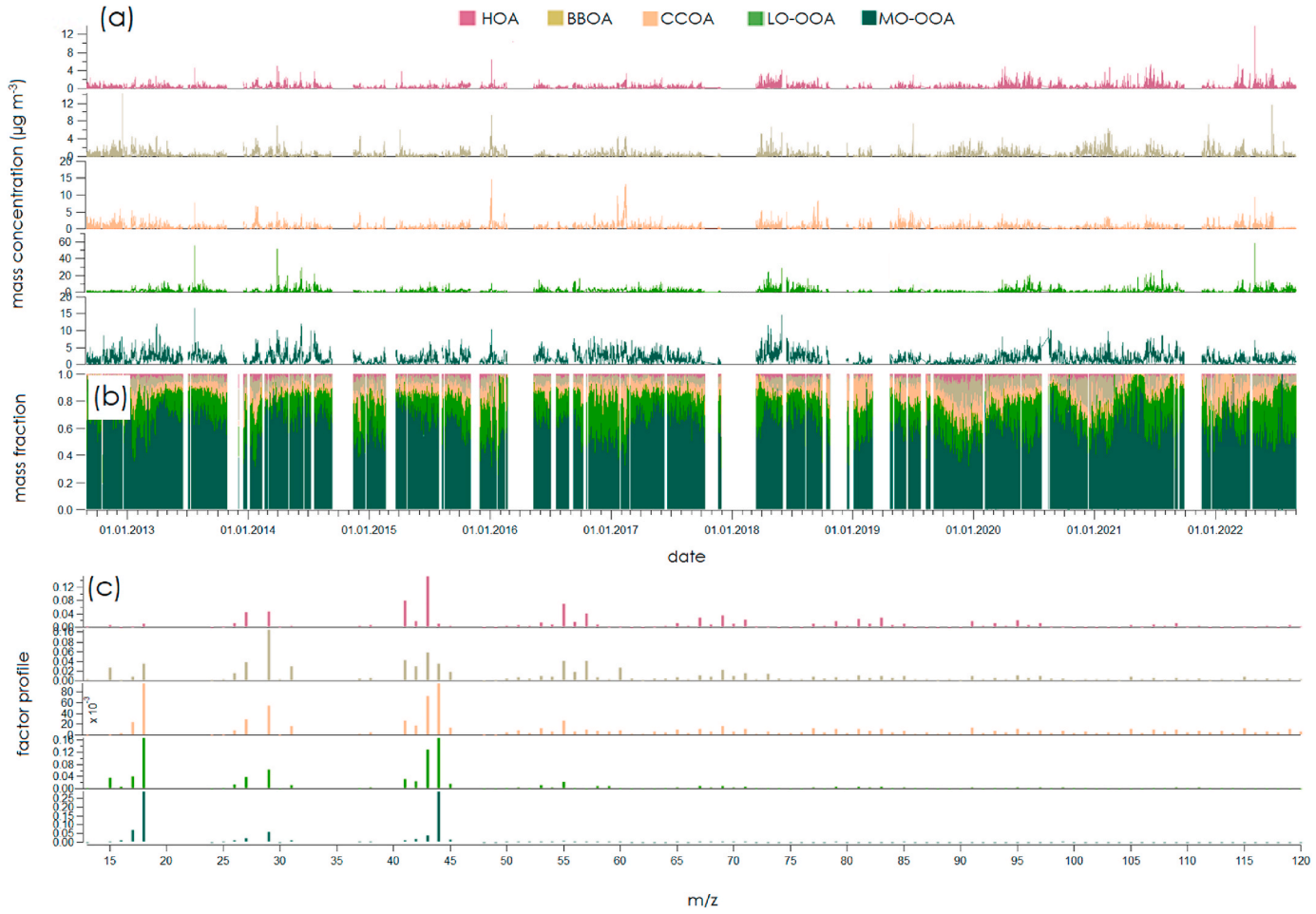

Fig. 5. (a) mass concentration, (b) mass contribution, and mass spectra of OA factors from rolling PMF model.

different seasons. Over a decade, this analysis of OA sources highlights the importance of primary and secondary sources in influencing the overall OA concentration and composition. The subsequent section (Sec. 3.2) will further explore the trends and implications of these OA sources across different seasons and air masses.

3.2.1. *Temporal and seasonal variation of OA PMF sources*

The year-to-year mean mass concentration and contribution of the PMF and eBC(PM_1) sources factors based on seasons and air masses are shown in Figs. 6 and 7, Figs. S7, and S8, with more details in Tables S4 and S5.

The results indicate that all OA and eBC(PM_1) source factors had

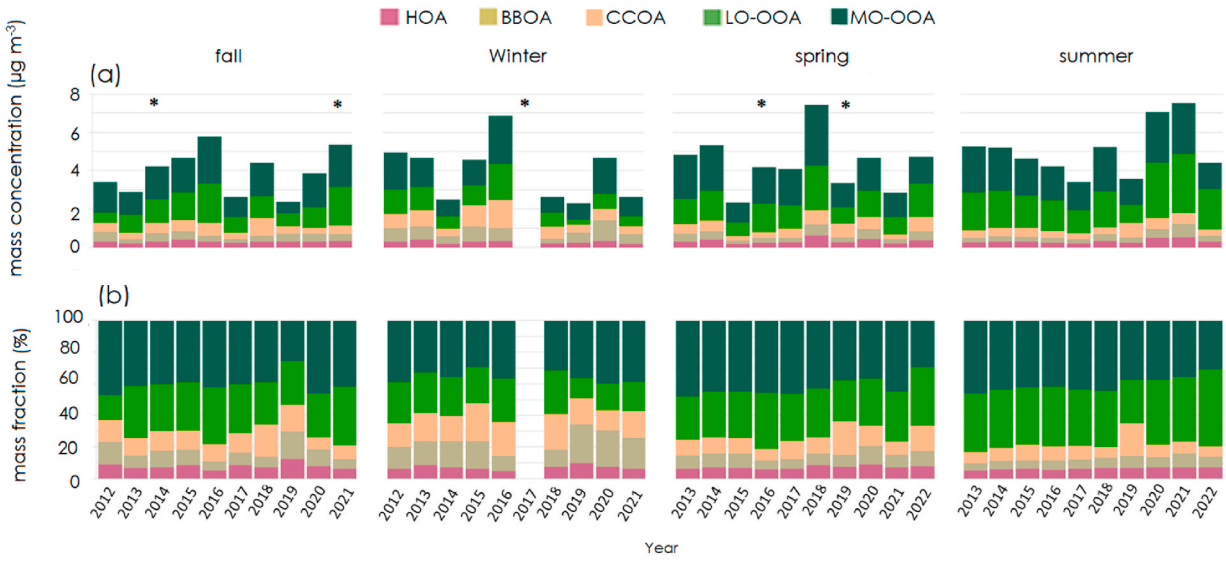

Fig. 6. (a) yearly mean mass concentration of the particulate OA sources, and (b) the corresponding mass contribution. Stars mean the data coverage is ≤ 1 month.

Fig. 7. Yearly mean mass concentration and mass contribution of the PMF factors for (a) Western air mass and (b) Eastern air mass for different meteorological seasons.

higher mass concentrations for Eastern airmasses, emphasizing the significant impact of long-range transported emissions in this region. Despite annual variations in total OA mass concentration within a given season (Figs. 6 and 7), a certain consistency in the distribution of the different PMF factors was observed, particularly during summer and spring. In these seasons, the distribution of sources remained relatively stable from year to year. Conversely, in fall and winter, there was more variability in the source distribution, which could be attributed to meteorological factors (such as temperature and precipitation) (Figs. S4 and S5) as well as varying contributions of Eastern and Western air masses during the same season. This seasonal and air mass dependency highlights the complex interplay between local meteorological conditions and the origin of air masses, affecting the composition and concentration of OA factors and eBC(PM_1) sources at the Melpitz site. These findings underscore the importance of considering both seasonal meteorological variations and air mass trajectories in understanding the sources and behavior of particulate matter in this region.

Hydrocarbon-like OA (HOA) contribution to total OA and eBC(PM_1) showed relatively stable percentages throughout the observation period, ranging from 5 % to 12 % and 1 %–4 %, respectively (Fig. 6). This stability can be attributed to household heating in cold seasons and central heating for hot water production across all seasons at the Melpitz station (Atabakhsh et al., 2023; van Pinxteren et al., 2024). These findings align with HOA contributions to total OA reported at other European sites, which range from 7.4 % to 12. 7 % (Chen et al., 2022). Despite the higher concentrations of HOA and eBC(PM_{1HOA}) in the Eastern air mass for all seasons (Fig. 7 and S8), their contributions did not show significant variability between the two air masses. In contrast, BBOA, CCOA, and their related eBC(PM_1) factors exhibited clear seasonality. Due to increased residential heating activities, their mass concentrations and contributions peaked during the colder months. BBOA and CCOA each contributed 24% to OA during the winter, comparable to other European sites where wintertime contributions range from 8.5 % to 25.3 % (Chen et al., 2022). During summer, BBOA and eBC (PM_{1BBOA}) were influenced by local heating systems, wildfire plumes, and recreative fires like barbecues and open fires (van Pinxteren et al., 2024). Although a fraction of CCOA and eBC(PM_{1CCOA}) might originate from nearby domestic heating, cf. van Pinxteren et al., 2024). Otherwise, these factors were generally associated with power plant emissions and long-distance transport throughout the year (Atabakhsh et al., 2023). The air mass classification results showed that POA factors, particularly BBOA, CCOA, and related eBC(PM_1) factors, dominated the OA and eBC (PM_1) mass concentrations and contributions during Eastern air masses in the winter season. This indicates that the origin of POA factors in cold seasons is likely linked to emissions transported from Eastern Europe, including countries such as the Eastern part of Germany, Poland, Czech Republic, and other further Eastern European nations.

Although factors associated with aged or processed OA (LO-OOA and MO-OOA) dominated the entire period (Fig. 7), these OOA factors made a higher contribution in summer during Eastern airmass (by an average of 41 % and 38 % of total OA), highlighting the influence of biogenic sources and LRT-aged particles from the Eastern side. Individually, the MO-OOA factor was likely driven by seasonal variation and LRT without a clear source identification. During the cold months, MO-OOA could be linked to aged POA resulting from heating activities. Additionally, as Gilardoni et al. (2016) suggested that aqueous-phase heterogeneous mechanisms might play a significant role in forming regional MO-OOAs during cold months. Higher values of MO-OOA in warm months might indicate the photochemical production of Secondary OA (SOA) particles (Petit et al., 2015)). Similarly, the LO-OOA factor, which shows a higher signal at m/z 43, could be related to different sources during cold and warm periods. During cold months and Eastern air masses, LO-OOA was

associated with aged residential heating factors (POA), which have recently been recognized as a significant source of oxidative potential in European fine aerosol (Daellenbach et al., 2020). Gas-particle partitioning also likely played a key role in LO-OOA formation during cold periods. In warmer months, LO-OOA tended to be associated with biogenic SOA, following the analysis by Chen et al. (2022), particularly in Eastern air masses. This indicated that the LO-OOA factor's sources and formation mechanisms vary significantly with season and air mass origin, reflecting the complex interplay between anthropogenic and biogenic emissions and atmospheric processing. Hence, clear differentiation between the two OOAs within the specified processes proved unattainable. This limitation can be attributed to the confined m/z range ($m/z < 120$) and/or the scarcity of organic tracers.

3.2.2. Trend analysis of OA PMF sources

The trend analysis of OA sources and eBC(PM_1)-related factors over a decade and seasons is presented in Fig. 8 and S8.

The HOA factor shows a small change in mass concentration during the considered decade, with -0.25 % y^{-1} (-0.002 μg m^{-3} y^{-1}) for the Eastern air mass, while it turned out to be not statistically significant for the entire period as well as Western air mass. This is consistent with previous studies, such as the SIRTA station (urban background), which also presented a negative trend (-0.05 μg m^{-3} y^{-1}; Zhang et al., 2019). Similarly, eBC(PM_{1HOA}) concentration displayed a significant, very small negative trend for all air masses over the decade (Fig. S8, Table S4). On a seasonal basis, HOA and eBC(PM_{1HOA}) both showed significant decreasing trends in winter, spring, and summer (Table S4). Conversely, an increasing trend was observed for HOA and eBC (PM_{1HOA}) concentrations during the fall. Regarding mass contribution to total OA, both HOA (Western -0.02 % y^{-1}) and eBC(PM_{1HOA}) (Western and entire; -0.06 % y^{-1} and -0.04 % y^{-1} respectively) showed a significant negative over the decade. However, a clear seasonality was noted: HOA contributions increased during fall (Western, entire, and Eastern: 0.11 % y^{-1}, 0.11 % y^{-1}, and 0.1 % y^{-1}) and summer (Western and entire: 0.05 % y^{-1} for both), while they decreased during winter (Western and entire: -0.11% y^{-1} and -0.05 % y^{-1} respectively) and spring (Western -0.11 % y^{-1}). Interestingly, the eBC(PM_{1HOA}) for summer has the only significant trend and behaves in the opposite direction than HOA (Western and entire: -0.03 % y^{-1} and -0.02 % y^{-1}, respectively). This seasonality suggests that, while HOA sources remain relatively stable throughout the year due to household heating and central heating for hot water production, their contributions and concentrations are influenced by seasonal variations. For example, increased HOA and eBC(PM_{1HOA}) during fall may be due to early residential heating activities. However, decreased concentrations during other seasons could result from reduced emissions and enhanced

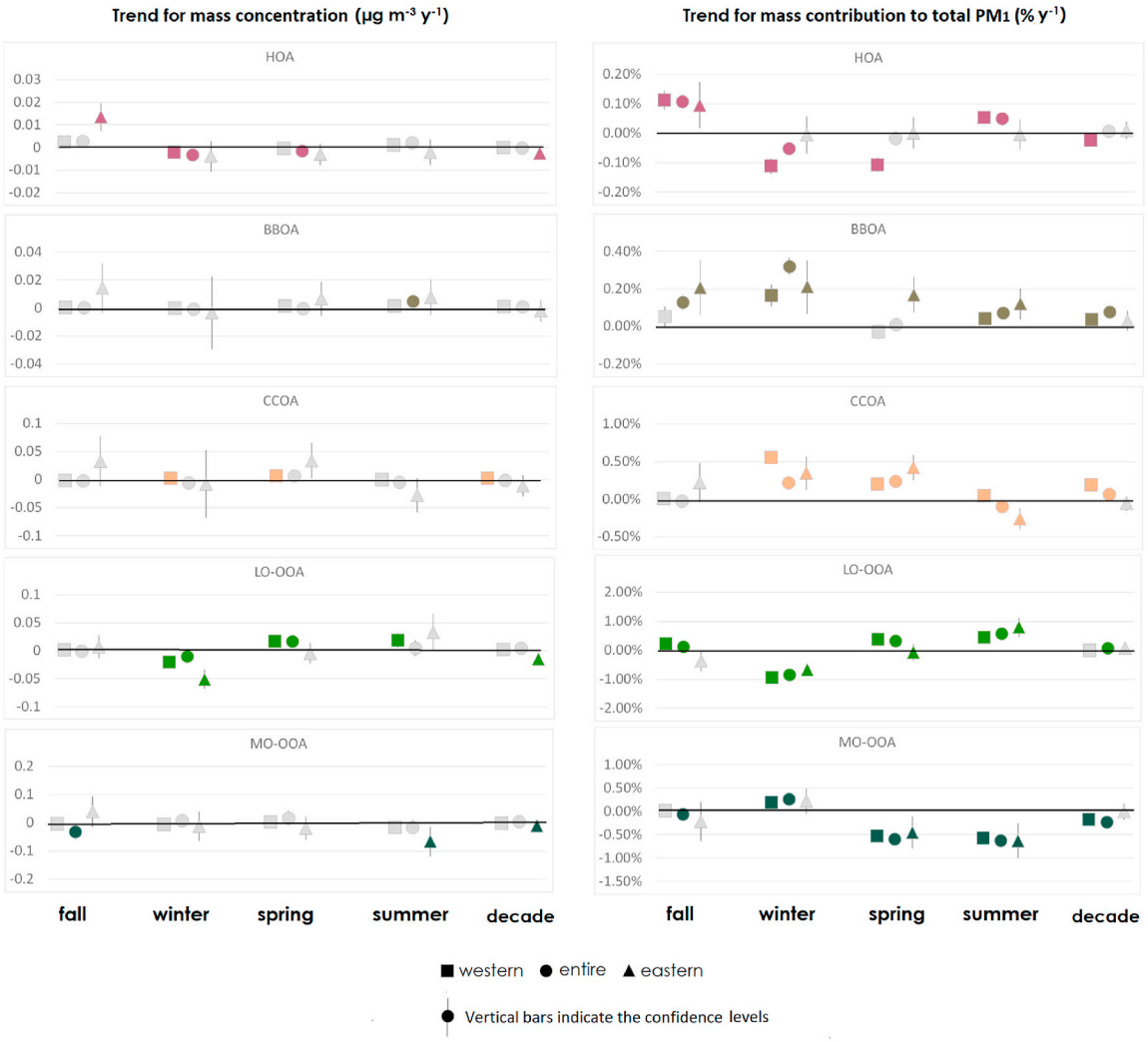

Fig. 8. Seasonal MK trend results for Melpitz station with long time series based on different seasons and the annual average for mass concentration and mass contribution of different organic sources. The colored symbols represent statistically significant, whereas grey symbols represent not statistically significant trends. The slope of the Western trend is shown by the square (■), entire by the circle (●), and Eastern by a triangle (▲), and vertical bars indicate the upper and lower confidence levels.

atmospheric dispersion and chemical processing. Overall, these findings highlight the complex dynamics of HOA and eBC(PM_{1HOA}), influenced by seasonal patterns and air mass origins. They reflect the interplay between local emissions, long-range transport, and meteorological conditions.

While the mass contribution of BBOA and eBC(PM_{1BBOA}) presented significant changes in this study (following discussion), their mass concentrations showed no significant trend over a decade. Only a small significant increase for BBOA and eBC(PM_{1BBOA}) concentration was observed during the summer (+0.004 μg m^{-3} y^{-1} and +0.002 μg m^{-3} y^{-1}, or +0.48 % y^{-1} and +0.25 % y^{-1}, respectively). This contrasts with findings from the SIRTA station, where a significant negative trend for BBOA was reported (−0.06 μg m^{-3} y^{-1}). The rise in BBOA and eBC (PM_{1BBOA}) during the summer in Melpitz is in line with wildfires and the temporary use of individual wood stoves. The survey results (van Pinxteren et al., 2024) indicated that one-third of the central heating systems, usually used for hot water generation, are wood-based. Regarding mass contributions, however, there were significant changes. The BBOA exhibited significant positive trends for the entire and Western air masses (+0.08 % y^{-1} and +0.04 % y^{-1}, respectively) in a decade, while the change for the Eastern air masses remains not statistically significant. Conversely, eBC(PM_{1BBOA}) showed positive trends for the Eastern (+0.2 % y^{-1}) and entire datasets (+0.08 % y^{-1}) and a negative trend for the Western air mass (−0.33 % y^{-1}) during the measurement period. Analyzing seasonal contribution trends, significant increases in slopes were observed for BBOA in the following cases: fall (entire +0.13 % y^{-1} and Eastern air masses +0.21 % y^{-1}), winter (Western, entire and East: +0.17 % y^{-1}, +0.31 % y^{-1}, and +0.21 % y^{-1} respectively), spring (Eastern air mass +0.17 % y^{-1}), and summer (Western, entire and Eastern: +0.04 % y^{-1}, +0.07 % y^{-1}, and +0.12 % y^{-1} respectively). For eBC(PM_{1BBOA}), significant increases in slopes were noted for fall (entire +0.35 % y^{-1}), winter (entire +0.13 % y^{-1}), and summer (entire +0.6% y^{-1} and Eastern +1.48 % y^{-1}). Conversely, significant decreases were found for winter (Western −0.7 % y^{-1}) and spring (entire and Western; −0.62 % y^{-1} and -0.79 % y^{-1}). These trends reflect the influence of various seasonal and regional factors, highlighting the importance of both local and regional sources in shaping the concentrations and contributions of BBOA and eBC(PM_{1BBOA}). In summary, analyzing the overall dataset alone may not accurately depict the true representation of changes in aerosol chemical composition. It is beneficial to consider specific air masses or direct wind patterns to ascertain from which sector the change is more pronounced, either positively or negatively.

The concentrations of CCOA and eBC(PM_{1CCOA}) factors exhibited a statistically significant small increase only during the Western air mass over the decade (+0.27 % y^{-1}, +0.1 % y^{-1}, respectively). Conversely, the slopes were not significant for the entire dataset as well as for the Eastern air mass over the decade. However, seasonal trends for the concentration of CCOA and eBC(PM_{1CCOA}) increased and decreased respectively during winter (Western +0.3 % y^{-1} and entire -0.17 % y^{-1} respectively) and increased in spring (Western +0.66 % y^{-1} and +0.27 % y^{-1} respectively, and entire for eBC(PM_{1CCOA}) +0.21% y^{-1}). Nevertheless, over the decade, contributions of both CCOA and eBC(PM_{1CCOA}) exhibited a positive trend for the Western air mass (+0.19 % y^{-1} and +0.38 % y^{-1}, respectively). The observed rise in the concentration and contribution of both CCOA and eBC(PM_{1CCOA}), especially in the Western regions, may be associated with recent shifts in the energy policies of coal-fired power plants (Alfie Shaw, 2023) and an increase in wildfires. Overall, the contribution of POA factors demonstrated significant and clear trend results, with increasing trends observed for BBOA, CCOA, and eBC(PM_1)-related factors most of the time. This underscores the growing importance of these two factors over the studied period.

The mass concentration of the LO-OOA factor exhibited a significant reduction in winter for all sectors: Western −2.04 % y^{-1} (−0.02 μg m^{-3} y^{-1}), entire −0.99 % y^{-1} (−0.009 μg m^{-3} y^{-1}), and East −5.1 % y^{-1} (−0.05 μg m^{-3} y^{-1}) and an increase in spring for the Western +1.73 % y^{-1} (+0.017 μg m^{-3} y^{-1}) and the entire +1.68 % y^{-1} (+0.016 μg m^{-3} y^{-1} respectively), as well as summer only for the Western +1.85 % y^{-1} (+0.018 μg m^{-3} y^{-1}). Over the decade, the trend was significant only for the Eastern air mass −1.52% y^{-1} (−0.015 μg m^{-3} y^{-1}). However, the remaining slopes were not statistically significant. Conversely, the trend result for LO-OOA mass contribution was significant for different seasons but not significant over the decade. Compared to the previous study, the SIRTA station (Zhang et al., 2019) showed no significant trend for LO-OOA. On the other hand, the mass concentration of MO-OOA was only significant during fall for the entire −3.12 % y^{-1} (−0.031 μg m^{-3} y^{-1}), summer East −6.62 % y^{-1} (−0.066 μg m^{-3} y^{-1}), and decade East −1.9 % y^{-1} (−0.01 μg m^{-3} y^{-1}); however, the MO-OOA contribution was significant most of the time, including fall (entire −0.06 % y^{-1}), winter (Western +0.2 % y^{-1} and entire +0.26 % y^{-1}), spring (Western −0.52 % y^{-1} and East −0.45 % y^{-1}), summer (all the sectors: Western −0.57 % y^{-1}, entire −0.62 % y^{-1}, and East −0.63 % y^{-1}), and over the decade (Western −0.17 % y^{-1} and entire −0.23 % y^{-1}). Compared to the previous study, the SIRTA station (Zhang et al., 2019) also exhibited a significant decreasing trend for MO-OOA (−0.17 μg m^{-3} y^{-1}). Since OOA sources are likely driven by meteorological conditions, seasons, long-range transport, and a variety of season-dependent formation mechanisms and sources (such as aged background, biomass burning, coal combustion, and biogenic sources), further investigation is required into the detailed OOA formation processes involved in this case to explain the trends observed in long-term measurements.

4. Conclusion

Over the past decade, the total PM_1 mass concentration at Melpitz has shown a significant decline of −4.59% y^{-1}, primarily driven by decreases in nitrate (−1.10% y^{-1}) and eBC(PM_1) (−1.3% y^{-1}) concentrations. These reductions highlight the impact of air pollution control strategies in Europe, particularly those targeting traffic-related emissions such as NOx and eBC(PM_1). Eastern European air masses consistently exhibited higher pollution levels compared to Western European ones, but this disparity decreased over time, indicating potential improvements in Eastern air quality. Sulfate concentrations showed no overall trend but exhibited seasonal variations, including an increase in summer due to new particle formation (NPF).

The trends in eBC(PM_1) and OA varied by season and air mass, reflecting the complexities of emission sources and atmospheric processes. Five OA factors—HOA, BBOA, CCOA, LO-OOA, and MO-OOA—contributed on average 7%, 10%, 12%, 31%, and 40% to OA, respectively. HOA concentrations (2% of eBC(PM_1)) remained stable overall, suggesting consistent local emissions, though a slight decrease was observed during Eastern air mass conditions (−0.25% y_{-1}). BBOA and CCOA (51% and 47% of eBC(PM_1); respectively) exhibited higher concentrations under Eastern air masses, indicating the influence of long-range transported emissions. BBOA contributions increased during winter (+0.32% over the decade), reflecting a growing reliance on biomass burning for residential heating. In contrast, CCOA showed an increasing trend under Western air mass conditions (+0.27% y^{-1}), potentially due to higher coal usage in Western European power plants. These results clearly emphasize the impact on European and national energy politics over the past decade, particularly the preference for biomass burning for house heating as a renewable energy source (European Union, 2023). Additionally, coal emissions associated with Western air masses have increased, potentially due to higher coal production from Western European coal power plants (IEA, 2023). The two OOAs (LO-OOA and MO-OOA) displayed distinct seasonal and spatial trends. LO-OOA had higher contributions in summer, driven by biogenic secondary organic aerosol (SOA) formation, and exhibited a significant decline in Eastern air masses (−1.52% y^{-1}). MO-OOA, often associated with long-range transport from Western Europe, also showed a significant Eastern decreasing trend (−1.09% y^{-1}), likely reflecting emission control strategies for anthropogenic SOA precursors. However, since the

precise origins of LO-OOA and MO-OOA (biogenic vs. anthropogenic) remain unclear, further research is needed to fully understand their sources and chemical properties.

Our results indicate the importance of investigating changes in mass concentration and changes in the distribution of sources or chemical species contributing to the total PM mass concentration. Such an approach is important not only for tracking the distribution of sources or chemical species in the particles but also for predicting the change in the aerosol's physical properties, such as hygroscopicity, light absorption, or scattering. The inclusion of such trends in prediction models could enhance our understanding of the long-term changes in aerosol particle properties and ultimately contribute to improvements in climate modeling.

CRediT authorship contribution statement

Samira Atabakhsh: Writing – original draft, Visualization, Validation, Software, Methodology, Investigation, Formal analysis, Data curation, Conceptualization. **Laurent Poulain:** Writing – review & editing, Validation, Supervision, Resources, Methodology. **Alessandro Bigi:** Writing – review & editing, Software, Methodology. **Martine Collaud Coen:** Writing – review & editing, Validation, Methodology. **Mira Pöhlker:** Writing – review & editing, Validation, Supervision, Resources. **Hartmut Herrmann:** Writing – review & editing, Validation, Supervision, Resources, Project administration.

Code availability

The SoFi code is the property of Datalystica and has been used under license. The ACSM data were analyzed using IGOR Pro 8.04 (Igor Pro, 2023; https://www.wavemetrics.com/). Source apportionment analysis was performed using SoFi 8.0.3.1 (https://datalystica.com/, SoFi pro, 2023, Canonaco et al., 2021). Backward trajectories were calculated using HYSPLIT-4 (https://www.ready.noaa.gov/HYSPLIT.php, NOAA Research, 2023; Draxler and Rolph, 2014). The code used to analyze the trend is available at https://github.com/mannkendall/R.

Funding

This research has been supported by the European Cooperation in Science and Technology (grant no. CA16109), ACTRIS (262254), and ACTRIS-2 (654109), and the H2020 Research Infrastructures (grant no. RI-URBANS (101036245)).

Declaration of competing interest

The authors declare that they have no known competing financial interests or personal relationships that could have appeared to influence the work reported in this paper.

Acknowledgments

This work is supported by the infrastructure projects ACTRIS (EU FP7; grant no. 262254) and ACTRIS-2 (grant no. 654109), the RI-URBANS project (grant no. 101036245).

Appendix A. Supplementary data

Supplementary data to this article can be found online at https://doi.org/10.1016/j.atmosenv.2025.121075.

Data availability

Data will be made available on request.

References

Alfie Shaw, 2023. European coal-fired power production rises 9% in September. https://www.power-technology.com/news/european-coal-production-increase-september/?cf-view.

Allan, J.D., Delia, A.E., Coe, H., Bower, K.N., Alfarra, M.R., Jimenez, J.L., Middlebrook, A.M., Drewnick, F., Onasch, T.B., Canagaratna, M.R., Jayne, J.T., Worsnop, D.R., 2004. A generalised method for the extraction of chemically resolved mass spectra from Aerodyne aerosol mass spectrometer data. J. Aerosol Sci. 35 (7), 909–922. https://doi.org/10.1016/j.jaerosci.2004.02.007.

Atabakhsh, S., Poulain, L., Chen, G., Canonaco, F., Prévôt, A.S.H., Pöhlker, M., Wiedensohler, A., Herrmann, H., 2023. A 1-year aerosol chemical speciation monitor (ACSM) source analysis of organic aerosol particle contributions from anthropogenic sources after long-range transport at the TROPOS research station Melpitz. Atmos. Chem. Phys. 23 (12), 6963–6988. https://doi.org/10.5194/acp-23-6963-2023.

Bigi, A., Vogt, F.P.A., 2021. mannkendall/R: bug fix: prob_mk_n. https://doi.org/10.5281/ZENODO.4495588.

Birmili, W., Stratmann, F., Wiedensohler, A., 1999. Technical note design of a dma-based size spectrometer for a large particle size range and stable operation. J. Aerosol Sci. 30 (Issue 4). https://doi.org/10.1016/S0021-8502(98)00047-0.

Birmili, W., Wiedensohler, A., 2000. New particle formation in the continental boundary layer: meteorological and gas phase parameter influence. Geophys. Res. Lett. 27 (20), 3325–3328. https://doi.org/10.1029/1999GL011221.

Bousiotis Pope, F.D., Beddows, D.C.S., Dall'Osto, M., Massling, A., Nøjgaard, J.K., Nordstrøm, C., Niemi, J.V., Portin, H., Petäjä, T., Perez, N., Alastuey, A., Querol, X., Kouvarakis, G., Mihalopoulos, N., Vratolis, S., Eleftheriadis, K., Wiedensohler, A., Weinhold, K., Merkel, M., Tuch, T., Harrison, R.M., 2021. A phenomenology of new particle formation (NPF) at 13 European sites. Atmos. Chem. Phys. 21 (15), 11905–11925. https://doi.org/10.5194/acp-21-11905-2021.

Bressi, M., Cavalli, F., Putaud, J.P., Fröhlich, R., Petit, J.E., Aas, W., Äijälä, M., Alastuey, A., Allan, J.D., Aurela, M., Berico, M., Bougiatioti, A., Bukowiecki, N., Canonaco, F., Crenn, V., Dusanter, S., Ehn, M., Elsasser, M., Flentje, H.M., Flentje, H., Graf, P., Green, D.C., Heikkinen, L., Hermann, H., Holzinger, R., Hueglin, C., Keernik, H., Kiendler-Scharr, A., Kubelova, L., Lunder, C., Maasikmets, M., Makes, O., Malaguti, A., Mihalopoulos, N., Nicolas, J.B., O'Dowd, C., Ovadnevaite, J., Petralia, E., Poulain, L., Priestman, M., Riffault, V., Ripoll, A., Schlag, P., Schwarz, J., Sciarec, J., Slowik, J., Sosedova, Y., Stavroulas, I., Teinemaa, E., Via, M., Vodickar, P., Williams, P.I., Wiedensohler, A., Young, D.E., Zhang, S., Favez, O., Minguillon, M.C., Prevot, A.S.H., 2021. A European aerosol phenomenology - 7: high-time resolution chemical characteristics of submicron particulate matter across Europe. Atmos. Environ. X 10. https://doi.org/10.1016/j.aeaoa.2021.100108.

Canonaco, F., Crippa, M., Slowik, J.G., Baltensperger, U., Prévôt, A.S.H., 2013. SoFi, an IGOR-based interface for the efficient use of the generalized multilinear engine (ME-2) for the source apportionment: ME-2 application to aerosol mass spectrometer data. Atmos. Meas. Tech. 6 (12), 3649–3661. https://doi.org/10.5194/amt-6-3649-2013.

Canonaco, F., Tobler, A., Chen, G., Sosedova, Y., Gates Slowik, J., Bozzetti, C., Rudolf Daellenbach, K., El Haddad, I., Crippa, M., Huang, R.J., Furger, M., Baltensperger, U., Prévôt, A.S.H., 2021. A new method for long-term source apportionment with time-dependent factor profiles and uncertainty assessment using SoFi Pro: application to 1 year of organic aerosol data. Atmos. Meas. Tech. 14 (2), 923–943. https://doi.org/10.5194/amt-14-923-2021.

Chebaicheb, H., de Brito, J.F., Chen, G., Tison, E., Marchand, C., Prévôt, A.S.H., Favez, O., Riffault, V., 2023. Investigation of four-year chemical composition and organic aerosol sources of submicron particles at the ATOLL site in northern France. Environmental Pollution 330. https://doi.org/10.1016/j.envpol.2023.121805.

Chen, G., Canonaco, F., Tobler, A., Aas, W., Alastuey, A., Allan, J., Atabakhsh, S., Aurela, M., Baltensperger, U., Bougiatioti, A., de Brito, J.F., Ceburnis, D., Chazeau, B., Chebaicheb, H., Daellenbach, K.R., Ehn, M., el Haddad, I., Eleftheriadis, K., Favez, O., Flentje, H., Font, A., Fossum, K., Freney, E., Gini, M., Green, D.C., Heikkinen, L., Herrmann, H., Kalogridis, A., Keernik, H., Lhotka, R., Lin, C., Lunder, C., Maasikmets, M., Manousakas, M.I., Marchand, N., Marin, C., Marmureanu, L., Mihalopoulos, N., Mocnika, G., Nęckia, J., O'Dowd, C., Ovadnevaite, J., Petera, T., Petita, J.E., Pikridasa, M., Matthew Platt, S., Pokorna, P., Poulain, L., Priestman, M., Riffault, V., Rinaldia, M., Rozanskia, K., Schwarz, J., Sciarea, J., Simon, L., Skiba, A., Slowik, J.G., Sosedova, Y., Stavroulas, I., Styszkoa, K., Teinemaa, E., Timonen, H., Tremper, A., Vasilescu, J., Via, M., Vodicka, P., Wiedensohler, A., Zografou, O., Cruz Minguillon, M., Prévôt, A.S.H., 2022. European aerosol phenomenology – 8: harmonised source apportionment of organic aerosol using 22 Year-long ACSM/AMS datasets. Environ. Int. 166. https://doi.org/10.1016/j.envint.2022.107325.

Chen, G., Sosedova, Y., Canonaco, F., Fröhlich, R., Tobler, A., Vlachou, A., Daellenbach, K.R., Bozzetti, C., Hueglin, C., Graf, P., Baltensperger, U., Slowik, J.G., El Haddad, I., Prévôt, A.S.H., 2021. Time-dependent source apportionment of submicron organic aerosol for a rural site in an alpine valley using a rolling positive matrix factorisation (PMF) window. Atmos. Chem. Phys. 21 (19), 15081–15101. https://doi.org/10.5194/acp-21-15081-2021.

Chen, Z.Y., Petetin, H., Méndez Turrubiates, R.F., Achebak, H., Pérez García-Pando, C., Ballester, J., 2024. Population exposure to multiple air pollutants and its compound episodes in Europe. Nat. Commun. 15 (1). https://doi.org/10.1038/s41467-024-46103-3.

Collaud Coen, M., Andrews, E., Bigi, A., Romanens, G., Martucci, G., Vuilleumier, L., 2020b. Effects of the prewhitening method, the time granularity and the time segmentation on the Mann-Kendall trend detection and the associated Sen's slope. https://doi.org/10.5194/amt-2020-178.

Collaud Coen, M., Andrews, E., Alastuey, A., Arsov, T.P., Backman, J., Brem, B.T., Bukowiecki, N., Couret, C., Eleftheriadis, K., Flentje, H., Fiebig, M., Gysel-Beer, M., Hand, J.L., Hoffer, A., Hooda, R., Hueglin, C., Joubert, W., Keywood, M., Kim, J.E., Kim, S., Labuschagne, C., Lin, N., Lin, Y., Myhre, C.L., Luoma, K., Lyamani, H., Marinoni, A., Mayol-Bracero, O.L., Mihalopoulos, N., Pandolfi, M., Prats, N., Prenni, A.J., Putaud, J.P., Ries, L., Reisen, F., Sellegri, K., Sharma, S., Sheridan, P., Sherman, J.P., Sun, J., Titos, G., Torres, E., Tuch, T., Weller, R., Wiedensohler, A., Zieger, P., Laj, P., 2020a. Multidecadal trend analysis of in situ aerosol radiative properties around the world. Atmos. Chem. Phys. 20 (14), 8867–8908. https://doi.org/10.5194/acp-20-8867-2020.

Crenn, V., Sciare, J., Croteau, L., Verlhac, S., Fröhlich, R., Belis, A., Aas, W., Äijälä, M., Alastuey, A., Artíñano, B., Croteau, P. L., Belis, C. A., Artiñano, B., Baisnée, D., Bonnaire, N., Bressi, M., Canagaratna, M., Canonaco, F., Carbone, C., Cavali, F., Coz, E. Cubison, M. J., Esser-Gietl, J. K., Green, D. C., Gros, V., Heikkinen, L., Herrmann, H., Lunder, C., Minguillon, M. C., Moncnik, G., O'dowd, C. D., Ovadnevaute, J., Perir, J.-E., Petralia, E., Poulain, L., Preiestman, M., Riffault, V., Ripoll, A., Sarda-Esteve, R., Slowik, J. G., Setyan, A., Wiedensohler, A., Baltensperger, U., Prevot, A. S. H., Jayne, J. T., Favez, O. (2015). ACTRIS ACSM intercomparison – Part 1: reproducibility of concentration and fragment results from 13 individual Quadrupole Aerosol Chemical Speciation Monitors (Q-ACSM) and consistency with co-located instruments. Eur. Geosci. Union, 8(12), 5063–5087. https://doi.org/10.5194/amt.

Crippa, M., Canonaco, F., Lanz, V.A., Äijälä, M., Allan, J.D., Carbone, S., Capes, G., Ceburnis, D., Dall'Osto, M., Day, D.A., DeCarlo, P.F., Ehn, M., Eriksson, A., Freney, E., Hildebrandt Ruiz, L., Hillamo, R., Jimenez, J.L., Junninen, H., Kiendler-Scharr, A., Kortelainen, A.-M., Kulmala, M., Laaksonen, A., Mensah, A.A., Mohr, C., Nemitz, E., O'Dowd, C., Ovadnevaite, J., Pandis, S.N., Petäjä, T., Poulain, L., Saarikoski, S., Sellegri, K., Swietlicki, E., Tiitta, P., Worsnop, D.R., Baltensperger, U., Prévôt, A.S.H., 2014. Organic aerosol components derived from 25 AMS data sets across Europe using a consistent ME-2 based source apportionment approach. Atmos. Chem. Phys. 14 (12), 6159–6176. https://doi.org/10.5194/acp-14-6159-2014.

Cusack, M., Alastuey, A., Pérez, N., Pey, J., Querol, X., 2012. Trends of particulate matter (PM 2.5) and chemical composition at a regional background site in the Western Mediterranean over the last nine years (2002-2010). Atmos. Chem. Phys. 12 (18), 8341–8357. https://doi.org/10.5194/acp-12-8341-2012.

Daellenbach, K.R., Uzu, G., Jiang, J., Cassagnes, L.E., Leni, Z., Vlachou, A., Stefenelli, G., Canonaco, F., Weber, S., Segers, A., Kuenen, J.J.P., Schaap, M., Favez, O., Albinet, A., Aksoyoglu, S., Dommen, J., Baltensperger, U., Geiser, M., el Haddad, I., Jaffrezo, J.L., Prévôt, A.S.H., 2020. Sources of particulate-matter air pollution and its oxidative potential in Europe. Nature 587 (7834), 414–419. https://doi.org/10.1038/s41586-020-2902-8.

Draxler, R.R., Rolph, G.D., 2014. HYSPLIT (HYbrid Single-Particle Lagrangian Integrated Trajectory) Model Access via NOAA ARL READY Website, NOAA Air Resources Laboratory. Silver Spring, USA.

European Environment Agency, 2023. Air pollutant emissions data viewer (gothenburg protocol, air convention) 1990-2021 — European environment agency. https://www.eea.europa.eu/data-and-maps/dashboards/air-pollutant-emissions-data-viewer-5.

European environment Agency, 2023. Harm to human health from air pollution in Europe: burden of disease 2023 — European Environment Agency. https://www.eea.europa.eu/publications/harm-to-human-health-from-air-pollution/.

European Parliament and Council of the European Union, 2008. Directive - 2008/50 - EN - EUR-lex. https://eur-lex.europa.eu/eli/dir/2008/50/oj.

European Union, 2023. Biomass. https://energy.ec.europa.eu/topics/renewable-energy/bioenergy/biomass_en.

Fowler, D., Pilegaard, K., Sutton, M., Ambus, P., Raivonen, M., Duyzer, J., Simpson, D., Fagerli, H., Fuzzi, S., Schjoerring, J., Granier, C., Neftel, A., Isaksen, I., Laj, P., Maione, M., Monks, P., Burkhardt, J., Daemmgen, U., Neirynck, J., Personne, E., Wichink-Kruit, R., Butterbach-Bahl, K., Flechard, C., Tuovinen, J., Coyle, M., Gerosa, G., Loubet, B., Altimir, N., Gruenhage, L., Ammann, C., Cieslik, S., Paoletti, E., Mikkelsen, T., Ro-Poulsen, H., Cellier, P., Cape, J., Horváth, L., Loreto, F., Niinemets, Ü., Palmer, P., Rinne, J., Misztal, P., Nemitz, E., Nilsson, D., Pryor, S., Gallagher, M., Vesala, T., Skiba, U., Brüggemann, N., Zechmeister-Boltenstern, S., Williams, J., O'Dowd, C., Facchini, M., de Leeuw, G., Flossman, A., Chaumerliac, N., Erisman, J., 2009. Atmospheric composition change: ecosystems-Atmosphere interactions. In: Atmospheric Environment, vol. 43. Elsevier Ltd, pp. 5193–5267. https://doi.org/10.1016/j.atmosenv.2009.07.068, 33.

Gilardoni, S., Massoli, P., Paglione, M., Giulianelli, L., Carbone, C., Rinaldi, M., Decesari, S., Sandrini, S., Costabile, F., Gobbi, G.P., Pietrogrande, M.C., Visentin, M., Scotto, F., Fuzzi, S., Facchini, M.C., 2016. Direct observation of aqueous secondary organic aerosol from biomass-burning emissions. Proceedings of the National Academy of Sciences of the United States of America 113 (36), 10013–10018. https://doi.org/10.1073/pnas.1602212113.

Hirsch, R.M., Slack, J.R., Smith, R.A., 1982. Techniques of trend analysis for monthly water quality data. WATER RESOURCES RESEARCH 18. https://doi.org/10.1029/WR018i001p00107.

IEA, 2023. Coal - iea. https://www.iea.org/energy-system/fossil-fuels/coal.

Igor Pro; Wavemetrics Inc, OR, USA, https://www.wavemetrics.com/, last access: 31. January 2025.

Iinuma, Y., Engling, G., Puxbaum, H., Herrmann, H., 2009. A highly resolved anion-exchange chromatographic method for determination of saccharidic tracers for biomass combustion and primary bio-particles in atmospheric aerosol. Atmos. Environ. 43 (6), 1367–1371. https://doi.org/10.1016/j.atmosenv.2008.11.020.

IPCC, 2021. Climate change 2021: the physical science basis | climate change 2021. The Physical Science Basis. https://www.ipcc.ch/report/ar6/wg1/.

Jayne, Danna C. Leard, Zhang, Xuefeng, Davidovits, Paul, Smith, Kenneth A., Kolb, Charles E., Worsnop, Douglas R., 2000. Development of an aerosol mass spectrometer for size and composition analysis of submicron particles enhanced reader. https://doi.org/10.1080/027868200410840.

Jimenez, J.L., Canagaratna, M.R., Donahue, N.M., Prévôt, A.S.H., Zhang, Q., Kroll, J.H., DeCarlo, P.F., Allan, J.D., Coe, H., Ng, N.L., Aiken, A.C., Docherty, K.S., Ulbrich, I. M., Grieshop, A.P., Robinson, A.L., Duplissy, J., Smith, J.D., Wilson, K.R., Lanz, V.A., Hueglin, C., Sun, Y.L., Tian, J., Laaksonen, A., Raatikainen, T., Rautiainen, J., Vaattovaara, P., Ehn, M., Kulmala, M., Tomlinson, J.M., Collins, D.R., Cubison, M.J., Dunlea, E.J., Huffman, J.A., Onasch, T.B., Alfarra, M.R., Williams, P.I., Bower, K., Kondo, Y., Schneider, J., Drewnick, F., Borrmann, S., Weimer, S., Demerjian, K., Salcedo, D., Cottrell, L., Griffin, R., Takami, A., Miyoshi, T., Hatakeyama, S., Shimono, A., Sun, J.Y., Zhang, Y.M., Dzepina, K., Kimmel, J.R., Sueper, D., Jayne, J. T., Herndon, S.C., Trimborn, A.M., Williams, L.R., Wood, E.C., Middlebrook, A.M., Kolb, C.E., Baltensperger, U., Worsnop, D.R., 2009. Evolution of organic aerosols in the atmosphere. Science 326, 1525–1529. https://doi.org/10.1126/science.1180353.

Kessinger, S., Minkos, A., Dauert, U., Feigenspan, S., Wallek, S., Schemmel, A. Hintergrund April 2024: Luftqualität 2023 (vorläufige Auswertung).

Kulkarni, A., Von Storch, H., 1995. Monte Carlo Experiments on the Effect of Serial Correlation on the Mann-Kendall Test of Trend. https://doi.org/10.1127/metz/4/1992/82.

Laborde, M., Crippa, M., Tritscher, T., Jurányi, Z., Decarlo, P.F., Temime-Roussel, B., Marchand, N., Eckhardt, S., Stohl, A., Baltensperger, U., Prévôt, A.S.H., Weingartner, E., Gysel, M., 2013. Black carbon physical properties and mixing state in the European megacity Paris. Atmospheric Chemistry and Physics 13 (11), 5831–5856. https://doi.org/10.5194/acp-13-5831-2013.

Liu, P.S.K., Deng, R., Smith, K.A., Williams, L.R., Jayne, J.T., Canagaratna, M.R., Moore, K., Onasch, T.B., Worsnop, D.R., Deshler, T., 2007. Transmission efficiency of an aerodynamic focusing lens system: comparison of model calculations and laboratory measurements for the aerodyne aerosol mass spectrometer. Aerosol. Sci. Technol. 41 (8), 721–733. https://doi.org/10.1080/02786820701422278.

Middlebrook, A.M., Bahreini, R., Jimenez, J.L., Canagaratna, M.R., 2012. Evaluation of composition-dependent collection efficiencies for the Aerodyne aerosol mass spectrometer using field data. Aerosol Science and Technology 46 (3), 258–271. https://doi.org/10.1080/02786826.2011.620041.

Ng, N.L., Herndon, S.C., Trimborn, A., Canagaratna, M.R., Croteau, P.L., Onasch, T.B., Sueper, D., Worsnop, D.R., Zhang, Q., Sun, Y.L., Jayne, J.T., 2011. An Aerosol Chemical Speciation Monitor (ACSM) for routine monitoring of the composition and mass concentrations of ambient aerosol. Aerosol. Sci. Technol. 45 (7), 780–794. https://doi.org/10.1080/02786826.2011.560211.

2023 NOAA Research. https://www.ready.noaa.gov/HYSPLIT.php.

Paatero, P., 1999. The multilinear engine—a table-driven, least squares program for solving multilinear problems, including the n-way parallel factor analysis model. J. Comput. Graph Stat. 8 (4), 854–888. https://doi.org/10.1080/10618600.1999.10474853.

Parworth, C., Fast, J., Mei, F., Shippert, T., Sivaraman, C., Tilp, A., Watson, T., Zhang, Q., 2015. Long-term measurements of submicrometer aerosol chemistry at the Southern Great Plains (SGP) using an Aerosol Chemical Speciation Monitor (ACSM). Atmospheric Environment 106, 43–55. https://doi.org/10.1016/j.atmosenv.2015.01.060.

Petit, J.-E., Favez, O., Sciare, J., Crenn, V., Sarda-Esteve, R., Bonnaire, N., Mocnik, G., Dupont, J.C., Haeffelin, M., Leoz-Garziandia, E., Sarda, R., Petit, J.-E., Favez, O., Sciare, J., Crenn, V., Sarda-Estève, R., Bonnaire, N., Močnik, G., Dupont, J.-C., Haeffelin, M., Leoz-Garziandia, E., 2015. Two years of near real-time chemical composition of submicron aerosols in the region of Paris using an Aerosol Chemical Speciation Monitor (ACSM) and a multi-wavelength Aethalometer. European Geosciences Union 15 (6), 2985–3005. https://doi.org/10.5194/acpd-14-24221-2014ï.

Petzold, A., Schönlinner, M., 2004. Multi-angle absorption photometry - a new method for the measurement of aerosol light absorption and atmospheric black carbon. J. Aerosol Sci. 35 (4), 421–441. https://doi.org/10.1016/j.jaerosci.2003.09.005.

Poulain, L., Spindler, G., Birmili, W., Plass-Dülmer, C., Wiedensohler, A., Herrmann, H., 2011. Seasonal and diurnal variations of particulate nitrate and organic matter at the IfT research station Melpitz. Atmos. Chem. Phys. 11 (24), 12579–12599. https://doi.org/10.5194/acp-11-12579-2011.

Poulain, L., Spindler, G., Grüner, A., Tuch, T., Stieger, B., Pinxteren, D. Van, Petit, J.E., Favez, O., Herrmann, H., Wiedensohler, A., 2020. Multi-year ACSM measurements at the central European research station Melpitz (Germany)-Part 1: instrument robustness, quality assurance, and impact of upper size cutoff diameter. Atmos. Meas. Tech. 13 (9), 4973–4994. https://doi.org/10.5194/amt-13-4973-2020.

Ren, Y., Stieger, B., Spindler, G., Grosselin, B., Mellouki, A., Tuch, T., Wiedensohler, A., Herrmann, H., 2020. Role of the dew water on the ground surface in HONO distribution: a case measurement in Melpitz. Atmos. Chem. Phys. 20 (21), 13069–13089. https://doi.org/10.5194/acp-20-13069-2020.

Spindler, G., Brüggemann, E., Gnauk, T., Grüner, A., Müller, K., Herrmann, H., 2010. A four-year size-segregated characterization study of particles PM10, PM2.5 and PM1 depending on air mass origin at Melpitz. Atmos. Environ. 44 (2), 164–173. https://doi.org/10.1016/j.atmosenv.2009.10.015.

Spindler, G., Gnauk, T., Grüner, A., Iinuma, Y., Müller, K., Scheinhardt, S., Herrmann, H., 2012. Size-segregated characterization of PM10 at the EMEP site Melpitz (Germany) using a five-stage impactor: a six year study. J. Atmos. Chem. 69 (2), 127–157. https://doi.org/10.1007/s10874-012-9233-6.

Spindler, G., Grüner, A., Müller, K., Schlimper, S., Herrmann, H., 2013. Long-term size-segregated particle (PM10, PM2.5, PM1) characterization study at Melpitz - influence of air mass inflow, weather conditions and season. J. Atmos. Chem. 70 (2), 165–195. https://doi.org/10.1007/s10874-013-9263-8.

Stieger, B., Spindler, G., Fahlbusch, B., Müller, K., Grüner, A., Poulain, L., Thöni, L., Seitler, E., Wallasch, M., Herrmann, H., 2018. Measurements of PM10 ions and trace gases with the online system MARGA at the research station Melpitz in Germany – a five-year study. J. Atmos. Chem. 75 (1), 33–70. https://doi.org/10.1007/s10874-017-9361-0.

Sun, J., Birmili, W., Hermann, M., Tuch, T., Weinhold, K., Merkel, M., Rasch, F., Müller, T., Schladitz, A., Bastian, S., Löschau, G., Cyrys, J., Gu, J., Flentje, H., Briel, B., Asbach, C., Kaminski, H., Ries, L., Sohmer, R., Gerwig, H., Wirtz, K., Meinhardt, F., Schwerin, A., Bath, O., Ma, N., Wiedensohler, A., 2020. Decreasing trends of particle number and black carbon mass concentrations at 16 observational sites in Germany from 2009 to 2018. Atmos. Chem. Phys. 20 (11), 7049–7068. https://doi.org/10.5194/acp-20-7049-2020.

Sun, Y., Xu, W., Zhang, Q., Jiang, Q., Canonaco, F., Prévôt, A.S.H., Fu, P., Li, J., Jayne, J., Worsnop, D.R., Wang, Z., 2018. Source apportionment of organic aerosol from 2-year highly time-resolved measurements by an aerosol chemical speciation monitor in Beijing, China. Atmos. Chem. Phys. 18 (12), 8469–8489. https://doi.org/10.5194/acp-18-8469-2018.

Tichý, O., Eckhardt, S., Balkanski, Y., Hauglustaine, D., Evangeliou, N., 2023. Decreasing trends of ammonia emissions over Europe seen from remote sensing and inverse modelling. Atmos. Chem. Phys. 23 (24), 15235–15252. https://doi.org/10.5194/acp-23-15235-2023.

Tobler, A., Skiba, A., Canonaco, F., Močnik, G., Rai, P., Chen, G., Bartyzel, J., Zimnoch, M., Styszko, K., Nęcki, J., Furger, M., Różański, K., Baltensperger, U., Slowik, J., Prévôt, A., 2021. Characterization of NR-PM_1 and source apportionment of organic aerosol in Krakow, Poland. Atmos. Chem. Phys. 1–22. https://doi.org/10.5194/acp-2021-197.

Tuch, T.M., Haudek, A., Nowak, A., Wex, H., Wiedensohler, A., 2009. Atmospheric Measurement Techniques Design and performance of an automatic regenerating adsorption aerosol dryer for continuous operation at monitoring sites. In *Atmos.* Meas. Tech 2.

Ulbrich, I.M., Canagaratna, M.R., Zhang, Q., Worsnop, D.R., Jimenez, J.L., 2009. Interpretation of organic components from Positive Matrix Factorization of aerosol mass spectrometric data. Atmos. Chem. Phys. 9. www.atmos-chem-phys.net/9/2891/2009/.

van Pinxteren, D., Engelhardt, V., Mothes, F., Poulain, L., Fomba, K.W., Spindler, G., Cuesta-Mosquera, A., Tuch, T., Müller, T., Wiedensohler, A., Löschau, G., Bastian, S., Herrmann, H., 2024. Residential wood combustion in Germany: a twin-site study of local village contributions to particulate pollutants and their potential health effects. ACS Environmental Au 4 (1), 12–30. https://doi.org/10.1021/acsenvironau.3c00035.

Velthof, G.L., van Bruggen, C., Groenestein, C.M., de Haan, B.J., Hoogeveen, M.W., Huijsmans, J.F.M., 2012. A model for inventory of ammonia emissions from agriculture in The Netherlands. Atmos. Environ. 46, 248–255. https://doi.org/10.1016/j.atmosenv.2011.09.075.

Wang, W., Chen, Y., Becker, S., Liu, B., 2015. Linear trend detection in serially dependent hydrometeorological data based on a variance correction Spearman rho method. Water (Switzerland) 7 (12), 7045–7065. https://doi.org/10.3390/w7126673.

Wehner, B., Philippin, S., Wiedensohler, A., 2002. Design and calibration of a thermodenuder with an improved heating unit to measure the size-dependent volatile fraction of aerosol particles. Aerosol Science 33. https://doi.org/10.1016/S0021-8502(02)00056-3.

WHO, 2019. WHO. L'IV Com Sàrl, Switzerland, vol. 8, p. 55, 5. https://www.who.int/news-room/events/detail/2019/02/12/default-calendar/expert-consultation-risk-communication-and-intervention-to-reduce-exposure-and-to-minimize-the-health-effects-of-air-pollution. (Accessed 19 August 2024).

Yue, S., Pilon, P., Phinney, B., Cavadias, G., 2002. The influence of autocorrelation on the ability to detect trend in hydrological series. Hydrol. Process. 16 (9), 1807–1829. https://doi.org/10.1002/hyp.1095.

Zhang, Y., Favez, O., Petit, J.E., Canonaco, F., Truong, F., Bonnaire, N., Crenn, V., Amodeo, T., Prévôt, A.S.H., Sciare, J., Gros, V., Albinet, A., 2019. Six-year source apportionment of submicron organic aerosols from near-continuous highly time-resolved measurements at SIRTA (Paris area, France). Atmos. Chem. Phys. 19 (23), 14755–14776. https://doi.org/10.5194/acp-19-14755-2019.

Zhu, Q., Huang, X.F., Cao, L.M., Wei, L.T., Zhang, B., He, L.Y., Elser, M., Canonaco, F., Slowik, J.G., Bozzetti, C., El-Haddad, I., Prévôt, A.S.H., 2018. Improved source apportionment of organic aerosols in complex urban air pollution using the multilinear engine (ME-2). Atmospheric Meas. Tech. 11 (2), 1049–1060. https://doi.org/10.5194/amt-11-1049-2018.

Trends of PM_1 aerosol chemical composition, carbonaceous aerosol, and source over the last ten years at Melpitz (Germany)

Samira Atabakhsh et al.

Corresponding author: Hartmut Herrmann (herrmann@tropos.de)

Fig. S1. Availability of dataset: grey (not available), green (available).

Table S1. Seasonal and yearly mass concentration of each ACSM species (µg m^{-3}).

Species	Avg.	fall	winter	spring	summer
Org	4.35	3.86	4.11	4.35	5.02
Nitrate	2.30	2.08	3.67	2.6	0.89
Sulphate	1.52	1.43	1.69	1.55	1.43
Ammonium	1.12	1	1.54	1.24	0.7
eBC(PM_1)	0.57	0.62	1.03	0.44	0.24
Chloride	0.02	0.01	0.06	0.01	0

Fig. S2. The availability of the dataset is based on the following categories: not available (grey), not classified (green), west (blue), and east (pink) for each year based on the number of days.

Table S2: Data availability based on number of days.

Season	Class	2012	2013	2014	2015	2016	2017	2018	2019	2020	2021	2022
fall	NA	7	34	64	30	24	44	53	7	7	59	
	Local	19	7	2	9	22	3	4	25	30	9	
	West	64	38	9	25	26	39	26	55	42	19	
	East	1	12	16	27	19	5	8	9	12	4	
winter	NA	7	36	14	22	8	90	30	11	5	3	
	Local	15	8	14	11	25	0	31	15	47	19	
	West	42	35	52	53	39	1	26	64	16	66	
	East	27	12	11	5	19	0	4	1	13	3	
spring	NA		1	9	30	73	5	15	61	5	5	12
	Local		35	28	15	6	20	27	7	21	23	25
	West		34	33	47	7	51	21	16	53	60	31
	East		22	22	0	6	16	29	8	13	4	24
summer	NA		24	13	20	27	13	20	35	25	11	1
	Local		15	19	7	10	16	22	17	13	32	23
	West		43	48	53	46	61	41	40	44	42	49
	East		10	12	12	9	2	9	0	10	7	19

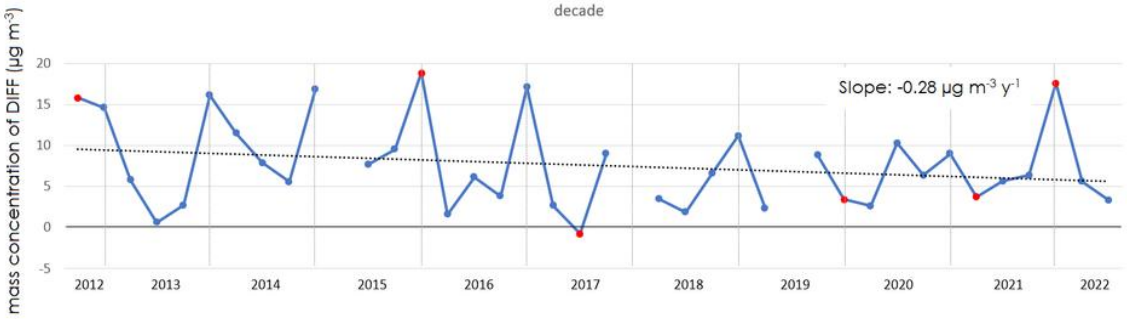

Fig. S3. The trend of DIFF (DIFF = mass concentration (East) – mass concentration (West)) of total PM_1 mass concentration over the decade, based on different years and seasons from the 3PW method. The red ones are the ones when the Eastern data contributions are less than 10% of the air mass classification.

Table S3. Seasonal and yearly mass concentration (μg m^{-3}) of each ACSM species, PMF factors, and eBC(PM_1)-related factors. Gray numbers are the data from the period with less than 50% data coverage.

Season	Year	Org	NO_3	SO_4	NH_4	eBC(PM_1)	HOA	BBOA	CCOA	LO-OOA	MO-OOA	eBC(PM_{1HOA})	eBC(PM_{1BBOA})	eBC(PM_{1CCOA})
fall	**2012**	3.2	2.1	1.4	1.0	0.7	0.3	0.4	0.4	0.5	1.6	0.01	0.2	0.1
	2013	2.8	1.6	0.9	0.8	0.5	0.1	0.2	0.3	0.9	1.2	0	0.1	0.1
	2014	4.0	1.6	1.8	0.8	0.6	0.3	0.4	0.4	1.2	1.6	0.01	0.2	0.1
	2015	5.6	5.0	2.4	2.4	1.0	0.4	0.4	0.5	1.4	1.8	0.01	0.2	0.2
	2016	5.5	1.9	1.7	1.0	0.7	0.3	0.3	0.6	2	2.4	0.01	0.1	0.2
	2017	2.6	1.3	1.1	0.6	0.4	0.2	0.2	0.3	0.8	1	0	0.1	0.1
	2018	4.4	1.3	1.1	0.6	0.5	0.3	0.3	0.8	1.1	1.7	0.01	0.1	0.3
	2019	2.2	1.6	0.7	0.5	0.5	0.2	0.4	0.3	0.6	0.6	0.01	0.2	0.1
	2020	3.6	1.5	0.9	0.6	0.5	0.3	0.4	0.2	1	1.7	0.01	0.2	0.1
	2021	6.2	3.8	2.2	1.9	0.4	0.3	0.3	0.4	2	2.2	0.01	0.1	0.1
winter	**2012**	4.8	4.1	2.0	1.8	1.3	0.3	0.6	0.7	1.2	1.9	0.01	0.3	0.2
	2013	4.7	3.2	1.6	1.4	1.3	0.4	0.7	0.8	1.1	1.5	0.01	0.3	0.3
	2014	2.4	3.2	1.6	1.3	0.9	0.1	0.4	0.3	0.6	0.8	0	0.2	0.1
	2015	4.4	4.2	1.4	1.5	1.1	0.2	0.7	1	1	1.3	0.01	0.4	0.4
	2016	6.2	3.8	2.3	2.0	1.3	0.3	0.6	1.4	1.8	2.5	0.01	0.3	0.5
	2017	6.7	4.8	2.5	2.1	1.5								
	2018	2.6	3.3	1.0	1.1	0.8	0.1	0.2	0.5	0.7	0.8	0	0.1	0.2
	2019	2.0	2.5	0.9	0.7	0.5	0.2	0.5	0.3	0.2	0.8	0	0.2	0.1
	2020	4.3	4.3	1.7	1.7	0.7	0.3	1	0.5	0.7	1.8	0.01	0.5	0.2
	2021	2.6	2.9	1.5	1.6	0.5	0.1	0.5	0.4	0.4	1	0	0.2	0.1
spring	**2013**	4.8	4.0	1.5	1.8	0.7	0.3	0.4	0.4	1.3	2.3	0.01	0.2	0.1
	2014	5.3	3.8	1.4	1.6	0.6	0.3	0.4	0.5	1.5	2.3	0.1	0.2	0.2
	2015	2.2	2.2	1.3	0.9	0.3	0.1	0.2	0.2	0.6	1	0	0.1	0.09
	2016	4.1	1.8	1.4	1.0	0.2	0.2	0.2	0.2	1.4	1.9	0	0.1	0.1
	2017	4.0	1.9	1.3	0.9	0.3	0.2	0.2	0.4	1.2	1.8	0	0.1	0.1
	2018	7.5	3.0	2.2	1.4	0.5	0.6	0.5	.7	2.3	3.1	0.02	0.2	0.2
	2019	3.3	1.8	1.2	0.8	0.2	0.2	0.2	0.6	0.8	1.2	0	0.1	0.3
	2020	4.3	2.1	1.4	0.8	0.4	0.4	0.5	0.5	1.3	1.7	0.01	0.2	0.2
	2021	2.8	2.7	1.0	1.1	0.3	0.2	0.2	0.2	0.9	1.2	0	0.1	0.08
	2022	4.4	1.6	2.3	1.4	0.3	0.3	0.4	0.7	1.7	1.4	0.01	0.2	0.2

Table S3 (continued).

Season	Year	Org	NO_3	SO_4	NH_4	eBC(PM_1)	HOA	BBOA	CCOA	LO-OOA	MO-OOA	eBC(PM_{1HOA})	eBC(PM_{1BBOA})	eBC(PM_{1CCOA})
summer	**2013**	5.3	1.2	0.9	0.7	0.3	0.2	0.2	0.3	1.9	2.4	0.01	0.1	0.1
	2014	5.1	1.3	0.9	0.6	0.3	0.3	0.3	0.4	1.9	2.2	0.01	0.1	0.1
	2015	4.5	1.7	1.2	0.9	0.2	0.2	0.2	0.4	1.7	1.9	0.01	0.1	0.1
	2016	4.2	1.1	0.7	0.4	0.2	0.2	0.2	0.3	1.5	1.7	0	0.1	0.1
	2017	3.6	1.2	0.6	0.4	0.2	0.2	0.2	0.2	1.2	1.5	0	0.1	0.1
	2018	5.2	1.3	0.7	0.6	0.2	0.3	0.3	0.3	1.8	2.3	0.01	0.1	0.1
	2019	3.5	0.9	0.8	0.4	0.1	0.2	0.2	0.7	0.9	1.3	0	0.1	0.2
	2020	6.6	1.2	0.7	0.5	0.1	0.5	0.4	0.5	2.8	2.6	0.01	0.2	0.2
	2021	7.4	1.5	1.2	1.0	0.1	0.5	0.6	0.5	3	2.6	0.01	0.3	0.2
	2022	4.1	0.8	2.3	1.1	0.2	0.3	0.3	0.2	2.1	1.3	0.01	0.1	0.1

Table S4. Seasonal and yearly mass concentration (μg m^{-3}) of each ACSM species, PMF factors, and eBC_PM_1-related factors for "Western air mass".

fall	HOA	BBOA	CCOA	LOOOA	MOOOA	eBC_HOA	eBC_BBOA	eBC_CCOA	Org	Nitrate	Ammonium	Sulphate	eBC
2012	0.30	0.44	0.43	0.52	1.33	0.01	0.23	0.17	2.81	1.70	0.79	1.19	0.64
2013	0.17	0.19	0.23	0.74	0.92	0.01	0.10	0.09	2.25	1.53	0.77	0.87	0.46
2014	0.17	0.32	0.24	0.74	0.92	0.00	0.05	0.06	1.50	1.27	0.76	1.58	0.24
2015	0.23	0.27	0.31	0.88	1.11	0.01	0.18	0.15	3.37	3.25	1.58	1.43	0.55
2016	0.21	0.24	0.41	1.34	1.68	0.01	0.12	0.16	3.68	1.83	0.80	1.09	0.49
2017	0.17	0.17	0.23	0.61	0.76	0.01	0.09	0.09	1.93	1.12	0.50	0.85	0.29
2018	0.23	0.23	0.67	0.88	1.18	0.01	0.12	0.27	3.24	0.96	0.43	0.78	0.37
2019	0.20	0.22	0.24	0.49	0.48	0.01	0.12	0.09	1.51	1.01	0.33	0.51	0.31
2020	0.21	0.26	0.17	0.73	1.32	0.01	0.13	0.07	2.55	1.15	0.48	0.66	0.34
2021	0.27	0.32	0.40	1.54	2.01	0.01	0.22	0.16	4.92	3.84	1.87	1.89	0.47
winter													
2012-2013	0.17	0.35	0.32	0.66	1.23	0.01	0.18	0.13	2.34	2.89	1.11	0.92	0.59
2013-2014	0.27	0.46	0.38	0.73	1.06	0.01	0.24	0.15	2.91	2.46	0.93	0.85	0.80
2014-2015	0.10	0.21	0.12	0.36	0.57	0.00	0.11	0.05	1.34	2.44	0.89	0.92	0.48
2015-2016	0.21	0.46	0.56	0.77	0.97	0.01	0.24	0.22	2.87	3.10	1.10	0.92	0.69
2016-2017	0.20	0.33	0.55	1.18	1.64	0.01	0.17	0.22	3.56	2.56	1.29	1.24	0.65
2017-2018									6.36	4.41	1.94	2.21	1.32
2018-2019	0.12	0.17	0.34	0.42	0.66	0.00	0.09	0.13	1.69	2.88	0.98	0.65	0.50
2019-2020	0.19	0.42	0.29	0.25	0.78	0.01	0.22	0.11	1.75	2.42	0.72	0.96	0.41

2020-2021	0.20	0.67	0.26	0.47	1.33	0.01	0.34	0.10	2.55	3.12	1.14	0.86	0.46
2021-2022	0.11	0.33	0.27	0.31	0.75	0.00	0.17	0.10	1.81	2.37	1.35	1.20	0.34

Table S4 (continued).

spring	**HOA**	**BBOA**	**CCOA**	**LOOOA**	**MOOOA**	**eBC_HOA**	**eBC_BBOA**	**eBC_CCOA**	**Org**	**Nitrate**	**Ammonium**	**Sulphate**	**eBC**
2013	0.20	0.22	0.24	0.76	1.56	0.01	0.11	0.09	2.99	3.27	1.31	0.96	0.44
2014	0.21	0.21	0.22	0.66	1.30	0.01	0.11	0.09	2.59	2.81	1.11	0.90	0.35
2015	0.13	0.14	0.17	0.56	0.90	0.00	0.07	0.07	1.87	1.83	0.79	1.21	0.25
2016	0.17	0.22	0.18	0.95	1.46	0.01	0.12	0.07	3.00	2.22	1.18	1.32	0.29
2017	0.20	0.19	0.39	0.93	1.49	0.01	0.10	0.15	3.10	1.98	0.87	1.14	0.29
2018	0.42	0.33	0.46	1.16	1.86	0.02	0.17	0.19	4.34	3.14	1.24	1.68	0.34
2019	0.21	0.20	0.53	0.67	1.09	0.01	0.11	0.21	2.74	1.77	0.79	1.12	0.19
2020	0.37	0.45	0.45	1.28	1.55	0.01	0.23	0.18	3.84	2.22	0.92	1.50	0.32
2021	0.15	0.18	0.17	0.56	1.07	0.01	0.11	0.07	2.14	2.44	1.02	0.92	0.27
2022	0.21	0.28	0.44	1.11	1.09	0.01	0.11	0.16	2.85	1.13	1.13	2.09	0.21
summer													
2013	0.26	0.21	0.31	1.67	2.29	0.01	0.11	0.12	4.77	0.96	0.79	1.27	0.34
2014	0.20	0.19	0.23	1.16	1.40	0.01	0.10	0.09	3.15	0.87	0.55	1.12	0.25
2015	0.24	0.21	0.34	1.43	1.57	0.01	0.11	0.14	3.70	1.14	0.83	1.46	0.23
2016	0.19	0.18	0.28	1.07	1.28	0.01	0.09	0.11	3.05	0.63	0.41	1.05	0.23
2017	0.20	0.19	0.25	1.09	1.38	0.01	0.10	0.10	3.35	0.68	0.43	1.22	0.23
2018	0.26	0.28	0.24	1.36	1.92	0.01	0.15	0.10	4.09	0.76	0.66	1.39	0.18
2019	0.20	0.25	0.55	0.73	1.01	0.01	0.13	0.22	2.76	0.75	0.39	0.88	0.15
2020	0.35	0.32	0.35	1.80	2.07	0.01	0.17	0.14	4.52	0.62	0.45	1.09	0.14
2021	0.38	0.45	0.40	2.05	2.30	0.01	0.24	0.16	5.59	1.16	1.01	1.49	0.17
2022	0.24	0.21	0.30	1.49	1.02	0.01	0.08	0.03	3.24	0.68	0.99	2.11	0.14

Table S5. Seasonal and yearly mass concentration (μg m^{-3}) of each ACSM species, PMF factors, and eBC_PM_1-related factors for "Eastern air mass".

fall	HOA	BBOA	CCOA	LOOOA	MOOOA	eBC_HOA	eBC_BBOA	eBC_CCOA	Org	Nitrate	Ammonium	Sulphate	eBC
2012	0.59	0.82	0.91	0.81	6.07	0.02	0.39	0.33	8.87	4.09	2.52	5.49	1.99
2013	0.28	0.31	0.50	1.34	1.82	0.01	0.16	0.20	4.25	1.43	0.90	1.22	0.80
2014	0.37	0.54	0.61	1.48	2.07	0.01	0.20	0.20	5.35	1.74	0.92	1.94	0.96
2015	0.55	0.65	0.81	1.87	2.46	0.02	0.40	0.37	7.10	5.58	2.76	2.95	1.31
2016	0.38	0.35	0.87	2.43	2.59	0.01	0.18	0.35	6.41	1.49	0.96	2.10	0.78
2017	0.54	0.34	0.86	1.80	2.64	0.02	0.18	0.34	6.19	2.45	1.23	2.76	1.05
2018	0.46	0.46	1.45	1.90	3.17	0.02	0.24	0.57	7.43	1.44	0.86	1.80	0.84
2019	0.63	1.12	1.12	1.13	0.96	0.02	0.59	0.44	4.86	3.31	1.18	1.69	1.44
2020	0.49	0.83	0.49	1.56	2.61	0.02	0.43	0.19	5.71	2.28	1.02	1.56	0.97
2021	0.47	0.29	0.59	2.56	2.49	0.03	0.37	0.35	12.10	1.86	1.57	3.28	0.53
winter													
2012-2013	0.51	1.15	1.40	2.49	2.99	0.02	0.60	0.56	8.53	5.35	2.67	3.54	2.38
2013-2014	0.72	1.40	2.23	2.34	2.67	0.03	0.72	0.88	9.45	5.10	2.58	3.97	2.95
2014-2015	0.51	1.42	1.70	1.65	2.20	0.02	0.74	0.67	7.34	5.48	2.59	4.11	3.44
2015-2016	0.64	2.33	3.64	2.24	2.86	0.02	1.19	1.41	11.20	7.14	2.82	3.23	3.14
2016-2017	0.60	1.21	3.75	2.71	3.47	0.02	0.63	1.49	10.55	5.42	3.08	4.62	2.75
2017-2018													
2018-2019	0.44	0.57	1.40	1.93	1.53	0.02	0.30	0.56	5.90	4.34	1.91	3.34	2.38
2019-2020	0.58	1.41	0.89	0.38	1.01	0.02	0.74	0.35	4.15	2.33	0.81	1.03	1.38
2020-2021	0.52	1.53	1.02	1.01	2.49	0.02	0.80	0.41	6.59	4.35	2.08	2.84	1.26
2021-2022	0.44	1.22	1.67	1.65	2.64	0.02	0.64	0.66	7.70	6.03	3.91	5.32	1.74
spring													
2013	0.41	0.54	0.71	1.98	2.51	0.01	0.28	0.28	6.16	3.66	1.93	1.87	1.13
2014	0.59	0.76	0.87	2.55	3.76	0.02	0.40	0.35	8.86	4.69	2.23	2.37	1.11

2015													
2016	0.34	0.30	0.41	2.01	2.52	0.01	0.16	0.16	5.53	1.12	0.92	1.66	0.39
2017	0.32	0.32	0.54	1.60	2.53	0.01	0.17	0.22	5.37	1.72	0.88	1.50	0.58
2018	0.73	0.64	0.73	2.83	3.74	0.02	0.33	0.29	8.76	1.75	1.06	2.14	0.50
2019	0.36	0.38	1.08	1.23	1.64	0.01	0.20	0.43	4.74	1.73	0.81	1.39	0.30
2020	0.57	0.88	1.05	1.60	2.26	0.02	0.46	0.42	5.79	2.44	0.80	1.54	0.86
2021	0.20	0.15	0.35	1.79	1.90	0.01	0.10	0.15	4.54	2.78	1.30	1.43	0.48
2022	0.45	0.59	0.94	1.63	1.57	0.02	0.25	0.36	5.23	2.53	1.98	2.54	0.74

Table S5 (continued).

summer	**HOA**	**BBOA**	**CCOA**	**LOOOA**	**MOOOA**	**eBC_HOA**	**eBC_BBOA**	**eBC_CCOA**	**Org**	**Nitrate**	**Ammonium**	**Sulphate**	**eBC**
2013	0.26	0.27	0.44	2.41	2.36	0.01	0.14	0.17	5.73	0.72	0.73	1.18	0.39
2014	0.59	0.51	0.69	3.18	3.94	0.02	0.27	0.28	8.78	1.31	1.02	2.25	0.47
2015	0.58	0.49	0.90	2.95	3.72	0.02	0.25	0.36	8.30	1.80	1.53	2.95	0.50
2016	0.42	0.44	0.62	3.19	3.27	0.02	0.22	0.24	7.86	1.15	0.67	1.48	0.36
2017	0.21	0.16	0.32	1.12	1.36	0.01	0.09	0.13	3.23	0.49	0.31	0.90	0.26
2018	0.41	0.47	0.29	2.81	2.53	0.01	0.25	0.12	6.47	0.73	0.53	0.97	0.25
2019													
2020	0.87	0.97	1.19	5.85	3.96	0.02	0.50	0.48	12.47	1.20	0.95	2.23	0.27
2021	0.92	0.95	0.89	4.98	3.54	0.02	0.49	0.35	11.34	1.14	0.84	1.53	0.24
2022	0.37	0.39	0.20	2.69	1.69	0.01	0.18	0.06	5.32	0.70	1.29	2.92	0.28

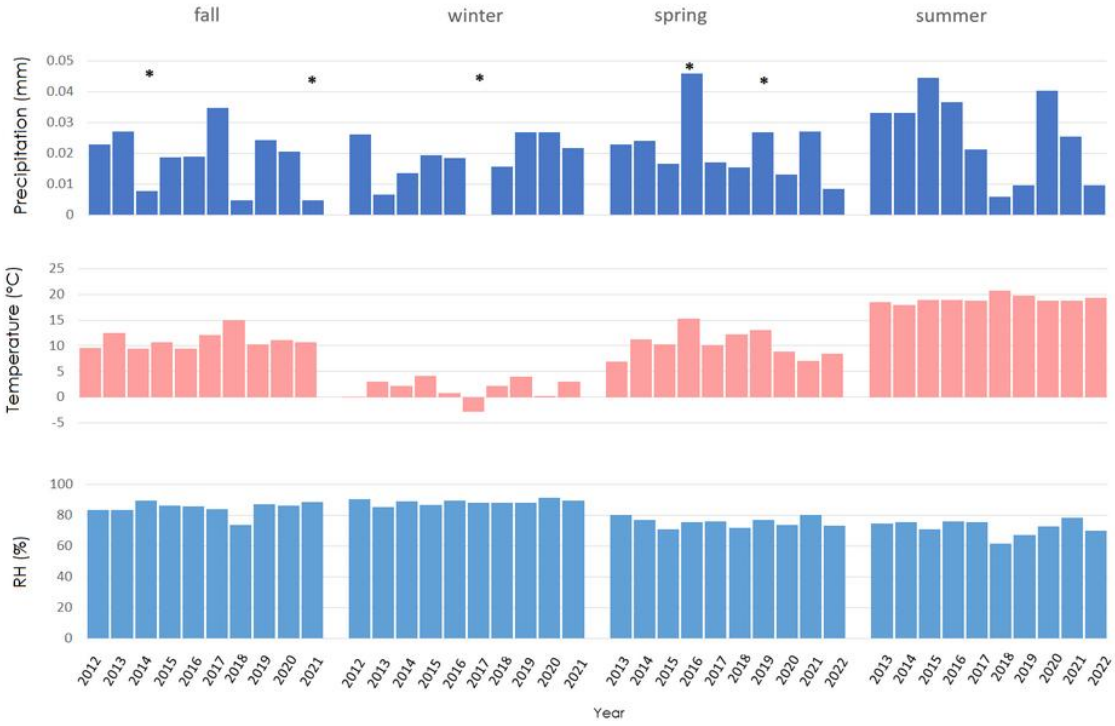

Fig. S4. Yearly mean precipitation, temperature, and relative humidity. Stars mean the data coverage is ≤ 1 month.

Fig. S5. Yearly mean mass concentration of (a) precipitation, (b) temperature, and (c) relative humidity.

Table S6: MK trends for "mass concentration" of all factors / chemicals in µg m^{-3} y^{-1} and percentage for decades and seasons, based on the "Western" air masses.

Season	Chemicals	Lower confident level		Slope		Upper confident level	
		µg m^{-3} y^{-1}	% y^{-1}	µg m^{-3} y^{-1}	% y^{-1}	µg m^{-3} y^{-1}	% y^{-1}
	Tot PM_1	-0.19	-18.66	-0.08	-8.41	0.02	1.82
fall	Org	-0.05	-4.79	-0.01	-0.84	-0.03	3.11
	Nitrate	-0.02	-2.42	0.01	1.09	0.05	4.61
	Sulfate	-0.05	-5.01	-0.04	-3.60	-0.02	-2.18
	Ammonium	-2.87	-2.87	-1.12	-1.12	0.63	0.63
	eBC(PM_1)	-0.01	-1.46	-0.01	-0.60	0.00	0.26
	HOA	0.00	0.02	0.00	0.25	0.00	0.48
	BBOA	0.00	-0.26	0.00	0.04	0.00	0.35
	CCOA	-0.01	-0.77	0.00	-0.14	0.00	0.49
	LO-OOA	-0.01	-0.80	0.00	0.18	0.01	1.14
	MO-OOA	-0.03	-2.63	0.00	-0.39	0.02	1.84
	eBC(PM_{1HOA})	0.00	0.00	0.00	0.01	0.00	0.01
	eBC(PM_{1BBOA})	0.00	-0.13	0.00	0.01	0.00	0.18
	eBC(PM_{1CCOA})	0.00	-0.29	0.00	-0.05	0.00	0.20
	Tot PM_1	-0.18	-18.40	-0.09	-8.78	0.01	0.87
winter	Org	-0.05	-5.11	-0.02	-2.41	0.00	0.28
	Nitrate	-0.07	-6.61	-0.02	-2.34	0.02	1.89
	Sulfate	-0.02	-1.84	-0.01	-0.58	0.01	0.67
	Ammonium	-0.03	-2.73	-0.01	-0.80	0.01	1.13
	eBC(PM_1)	-0.01	-1.17	0.00	-0.40	0.00	0.38
	HOA	0.00	-0.34	0.00	-0.21	0.00	-0.09
	BBOA	0.00	-0.24	0.00	-0.01	0.00	0.23
	CCOA	0.00	-0.07	0.00	0.30	0.01	0.68
	LO-OOA	-0.03	-2.50	-0.02	-2.04	-0.02	-1.58
	MO-OOA	-0.02	-1.86	0.00	-0.49	0.01	0.88
	eBC(PM_{1HOA})	0.00	-0.01	0.00	-0.01	0.00	0.00
	eBC(PM_{1BBOA})	0.00	-0.12	0.00	0.00	0.00	0.10
	eBC(PM_{1CCOA})	0.00	-0.04	0.00	0.11	0.00	0.25
	Tot PM_1	-0.08	-7.68	0.06	6.17	0.20	20.07
spring	Org	-0.03	-2.91	0.02	1.67	0.06	6.17
	Nitrate	-0.04	-3.93	0.02	1.61	0.07	7.18
	Sulfate	-0.01	-0.85	0.01	1.02	0.03	2.89
	Ammonium	-0.02	-1.9	0.01	0.53	0.03	2.96
	eBC(PM_1)	-0.01	-0.80	0.00	-0.16	0.00	0.49
	HOA	0.00	-0.21	0.00	-0.04	0.00	0.13
	BBOA	0.00	-0.05	0.00	0.16	0.00	0.38
	CCOA	0.00	0.21	0.01	0.66	0.01	1.11
	LO-OOA	0.01	0.88	0.02	1.73	0.03	2.57
	MO-OOA	-0.02	-1.86	0.00	0.27	0.02	2.40
	eBC(PM_{1HOA})	0.00	-0.01	0.00	0.00	0.00	0.00
	eBC(PM_{1BBOA})	0.00	-0.01	0.00	0.05	0.00	0.17
	eBC(PM_{1CCOA})	0.00	0.10	0.00	0.27	0.00	0.45
	Tot PM_1	-0.10	-10.30	0.00	0.22	0.11	10.74
summer	Org	-0.05	-5.47	0.00	-0.36	0.05	4.76
	Nitrate	-0.03	-3.11	-0.01	-1.00	0.01	1.11
	Sulfate	0.00	0.32	0.02	2.03	0.03	3.73
	Ammonium	0.00	-0.04	0.02	1.61	0.03	3.25
	eBC(PM_1)	-0.01	-0.66	0.00	-0.23	0.00	0.20
	HOA	0.00	-0.07	0.00	0.12	0.00	0.31
	BBOA	0.00	-0.07	0.00	0.15	0.00	0.36
	CCOA	0.00	-0.41	0.00	0.02	0.00	0.45
	LO-OOA	0.01	0.61	0.02	1.85	0.03	3.10
	MO-OOA	-0.04	-3.59	-0.01	-1.46	0.01	0.67
	eBC(PM_{1HOA})	0.00	0.00	0.00	0.00	0.00	0.01
	eBC(PM_{1BBOA})	0.00	-0.05	0.00	0.05	0.00	0.16
	eBC(PM_{1CCOA})	0.00	-0.18	0.00	-0.03	0.00	0.14

Table S6 (continued).

Season	Chemicals	Lower confident level		Slope		Upper confident level	
		µg m^{-3} y^{-1}	% y^{-1}	µg m^{-3} y^{-1}	% y^{-1}	µg m^{-3} y^{-1}	% y^{-1}
	Tot PM_1	-0.07	-6.86	-0.01	-1.46	0.04	3.94
decade	Org	-0.02	-2.05	0.00	-0.09	0.02	1.86
	Nitrate	-0.02	-2.06	0.00	-0.33	0.01	1.39
	Sulfate	-0.01	-0.78	0.00	-0.02	0.01	0.74
	Ammonium	-0.01	-0.73	0.00	0.21	0.01	1.15
	eBC(PM_1)	-0.01	-0.73	0.00	-0.42	0.00	-0.10
	HOA	0.00	-0.07	0.00	0.01	0.00	0.10
	BBOA	0.00	0.00	0.00	0.11	0.00	0.23
	CCOA	0.00	0.04	0.00	0.27	0.00	0.49
	LO-OOA	0.00	-0.18	0.00	0.22	0.01	0.63
	MO-OOA	-0.01	-1.08	0.00	-0.13	0.01	0.82
	eBC(PM_{1HOA})	0.00	0.00	0.00	0.00	0.00	0.00
	eBC(PM_{1BBOA})	0.00	0.00	0.00	0.04	0.00	0.10
	eBC(PM_{1CCOA})	0.00	0.01	0.00	0.10	0.00	0.19

Table S7: MK trends for "mass concentration" of all factors / chemicals in µg m^{-3} y^{-1} and percentage for decades and seasons, based on the "entire" dataset.

Season	Chemicals	Lower confident level		Slope		Upper confident level	
		µg m^{-3} y^{-1}	% y^{-1}	µg m^{-3} y^{-1}	% y^{-1}	µg m^{-3} y^{-1}	% y^{-1}
	Tot PM_1	-0.22	-22.05	-0.11	-11.07	0.00	-0.10
fall	Org	-0.06	-5.56	-0.02	-1.77	0.02	2.03
	Nitrate	-0.04	-4.32	-0.01	-0.54	0.03	3.23
	Sulfate	-0.06	-6.34	-0.04	-4.48	-0.03	-2.61
	Ammonium	-0.04	-4.31	-0.02	-2.35	0.00	-0.40
	eBC(PM_1)	-0.03	-3.13	0.02	-1.72	0.00	-0.32
	HOA	0.00	0.09	0.00	0.28	0.00	0.48
	BBOA	0.00	-0.37	0.00	0.06	0.00	0.48
	CCOA	-0.01	-0.94	0.00	-0.15	0.01	0.63
	LO-OOA	-0.01	-1.12	0.00	0.01	0.01	1.13
	MO-OOA	-0.06	-5.77	-0.03	-3.12	0.00	-0.49
	eBC(PM_{1HOA})	0.00	0.00	0.00	0.01	0.00	0.02
	eBC(PM_{1BBOA})	0.00	-0.13	0.00	0.07	0.00	0.27
	eBC(PM_{1CCOA})	0.00	-0.20	-0.03	-0.03	0.00	0.12
	Tot PM_1	-0.24	-23.61	-0.13	-12.73	-0.02	-1.85
winter	Org	-0.09	-9.94	-0.06	-6.17	-0.03	-3.30
	Nitrate	-0.07	-7.09	-0.02	-2.30	0.02	2.46
	Sulfate	-0.04	-4.17	-0.02	-2.45	-0.01	-0.73
	Ammonium	-0.03	-3.01	-0.01	-0.80	0.01	1.41
	eBC(PM_1)	-0.03	-3.19	-0.02	-1.77	0.00	-0.35
	HOA	0.00	-0.43	0.00	-0.30	0.00	-0.18
	BBOA	0.00	-0.45	0.00	-0.06	0.00	0.34
	CCOA	-0.01	-1.10	-0.01	-0.53	0.00	0.05
	LO-OOA	-0.02	-1.61	-0.01	-0.99	0.00	-0.38
	MO-OOA	-0.01	-0.90	0.01	0.93	0.03	2.76
	eBC(PM_{1HOA})	0.00	-0.01	0.00	-0.01	0.00	-0.01
	eBC(PM_{1BBOA})	0.00	-0.18	0.00	0.00	0.00	0.17
	eBC(PM_{1CCOA})	0.00	-0.29	0.00	-0.17	0.00	-0.05
	Tot PM_1	-0.19	-19.21	-0.06	-6.17	0.07	6.87
spring	Org	-0.07	-6.59	-0.02	-2.26	-0.02	2.07
	Nitrate	-0.09	-8.94	-0.04	-4.15	0.01	0.62
	Sulfate	-0.02	-2.19	0.00	-0.17	0.02	1.86
	Ammonium	-0.04	-3.50	-0.01	-1.24	0.01	1.02
	eBC(PM_1)	-0.03	-2.68	-0.02	-1.66	-0.01	-0.64
	HOA	0.00	-0.29	0.00	-0.14	0.00	0.01
	BBOA	0.00	-0.35	0.00	-0.03	0.00	0.29
	CCOA	0.00	0.12	0.01	0.71	0.01	1.31
	LO-OOA	0.01	0.75	0.02	1.68	0.03	2.62
	MO-OOA	-0.01	-0.83	0.02	1.70	0.04	4.23
	eBC(PM_{1HOA})	0.00	-0.01	0.00	-0.01	0.00	0.00
	eBC(PM_{1BBOA})	0.00	-0.13	0.00	0.00	0.00	0.14
	eBC(PM_{1CCOA})	0.00	0.09	0.00	0.21	0.00	0.34

Table S7 (continued).

Season	Chemicals	Lower confident level		Slope		Upper confident level	
		µg m^{-3} y^{-1}	% y^{-1}	µg m^{-3} y^{-1}	% y^{-1}	µg m^{-3} y^{-1}	% y^{-1}
	Tot PM_1	-0.04	-4.12	0.07	6.61	0.17	17.33
summer	Org	-0.04	-4.47	0.01	0.56	0.06	5.59
	Nitrate	0.00	-0.07	0.02	1.97	0.04	4.02
	Sulfate	0.00	0.49	0.03	2.51	0.05	4.52
	Ammonium	0.01	0.91	0.03	2.58	0.04	4.25
	eBC(PM_1)	-0.01	-1.00	0.00	-0.38	0.00	0.24
	HOA	0.00	0.06	0.00	0.22	0.00	0.38
	BBOA	0.00	0.18	0.00	0.48	0.00	0.78
	CCOA	-0.01	-0.99	0.00	-0.44	0.00	0.11
	LO-OOA	-0.01	-0.87	0.01	0.51	0.02	1.91
	MO-OOA	-0.04	-3.96	-0.01	-1.47	0.01	1.03
	eBC(PM_{1HOA})	0.00	0.00	0.00	0.00	0.00	0.01
	eBC(PM_{1BBOA})	0.00	0.10	0.00	0.25	0.00	0.39
	eBC(PM_{1CCOA})	0.00	-0.10	0.00	-0.02	0.00	-0.04
	Tot PM_1	-0.10	-10.25	-0.05	-4.59	0.01	1.07
Decade	Org	-0.04	-4.00	-0.02	-2.05	0.00	-0.10
	Nitrate	-0.03	-2.88	-0.01	-1.10	0.01	0.67
	Sulfate	-0.02	-1.93	-0.01	-0.99	0.00	-0.04
	Ammonium	-0.01	-1.31	0.00	-0.32	0.01	0.68
	eBC(PM_1)	-0.02	-1.81	-0.01	-1.30	-0.01	-0.78
	HOA	0.00	-0.09	0.00	-0.02	0.00	0.06
	BBOA	0.00	-0.06	0.00	0.12	0.00	0.29
	CCOA	0.00	-0.42	0.00	-0.11	0.00	0.19
	LO-OOA	0.00	0.01	0.00	0.50	0.01	0.98
	MO-OOA	-0.01	-0.70	0.00	0.45	0.02	1.61
	eBC(PM_{1HOA})	0.00	-0.01	0.00	0.00	0.00	0.00
	eBC(PM_{1BBOA})	0.00	0.00	0.00	0.07	0.00	0.16
	eBC(PM_{1CCOA})	0.00	-1.13	0.00	-0.42	0.00	0.29

Table S8: MK trends for "mass concentration" of all factors / chemicals in µg m^{-3} y^{-1} and percentage for decades and seasons, based on the "Eastern" air mass.

Season	Chemicals	Lower confident level		Slope		Upper confident level	
		µg m^{-3} y^{-1}	% y^{-1}	µg m^{-3} y^{-1}	% y^{-1}	µg m^{-3} y^{-1}	% y^{-1}
	Tot PM_1	-0.13	-13.28	0.22	22.12	0.58	57.53
fall	Org	0.02	1.85	0.14	13.80	0.26	25.90
	Nitrate	-0.11	-11.17	0.01	0.97	0.13	12.95
	Sulfate	-0.11	-10.80	-0.03	-2.67	0.05	5.41
	Ammonium	-0.09	-8.70	-0.02	-1.97	0.05	4.83
	eBC(PM_1)	-0.07	-7.01	0.01	1.12	0.09	9.36
	HOA	0.01	0.74	0.01	1.35	0.02	1.95
	BBOA	0.00	-0.34	0.01	1.42	0.03	3.20
	CCOA	-0.01	-1.11	0.03	3.31	0.08	7.72
	LO-OOA	-0.01	-1.34	0.03	0.68	0.01	2.74
	MO-OOA	-0.-1	-1.40	0.04	3.90	0.09	9.30
	eBC(PM_{1HOA})	0.00	0.04	0.00	0.05	0.00	0.07
	eBC(PM_{1BBOA})	0.00	-0.19	0.01	0.72	0.02	1.62
	eBC(PM_{1CCOA})	0.00	-0.39	0.01	1.30	0.03	3.00
	Tot PM_1	-0.58	-57.55	-0.10	-10.40	0.37	36.90
winter	Org	-0.19	-19.40	-0.07	-6.78	0.06	5.95
	Nitrate	-0.38	-37.61	-0.18	-17.84	0.02	1.98
	Sulfate	-0.11	-11.41	0.00	0.04	0.12	11.60
	Ammonium	-0.13	-12.88	0.06	-3.32	-0.03	6.30
	eBC(PM_1)	-0.26	-25.89	-0.14	-13.96	-0.02	-1.81
	HOA	-0.01	-1.07	0.00	-0.39	0.00	0.29
	BBOA	-0.03	-2.91	0.00	-0.34	0.02	2.25
	CCOA	-0.07	-6.73	-0.01	-0.75	0.05	5.23
	LO-OOA	-0.07	-6.79	-0.05	-5.10	-0.03	-3.41
	MO-OOA	-0.06	-6.33	-0.01	-1.20	0.04	3.92
	eBC(PM_{1HOA})	0.00	-0.03	0.00	-0.01	0.00	0.01
	eBC(PM_{1BBOA})	-0.01	-1.44	0.00	-0.14	0.01	1.16
	eBC(PM_{1CCOA})	-0.02	-2.49	0.00	-0.21	0.02	2.08

Table S8 (continued).

Season	Chemicals	Lower confident level		Slope		Upper confident level	
		μg m^{-3} y^{-1}	% y^{-1}	μg m^{-3} y^{-1}	% y^{-1}	μg m^{-3} y^{-1}	% y^{-1}
	Tot PM_1	-0.15	-15.29	0.16	15.05	0.47	46.99
spring	Org	-0.08	-8.40	0.02	2.45	0.13	13.34
	Nitrate	-0.09	-9.14	0.01	1.37	0.12	11.86
	Sulfate	-0.02	-1.89	0.04	3.83	0.10	9.55
	Ammonium	-0.02	-2.45	0.03	2.83	0.08	8.15
	eBC(PM_1)	-0.06	-5.83	-0.01	-1.23	0.03	3.30
	HOA	-0.01	-0.76	0.00	-0.30	0.00	0.15
	BBOA	-0.01	-0.59	0.01	0.65	0.02	1.87
	CCOA	0.00	0.23	0.03	3.39	0.07	6.56
	LO-OOA	-0.02	-2.18	0.00	-0.43	0.01	1.31
	MO-OOA	-0.06	-5.89	-0.02	-1.85	0.02	2.13
	eBC(PM_{1HOA})	0.00	-0.03	0.00	-0.02	0.00	-0.01
	eBC(PM_{1BBOA})	0.00	-0.27	0.00	0.33	0.00	0.95
	eBC(PM_{1CCOA})	0.00	0.10	0.01	1.31	0.03	2.51
	Tot PM_1	-0.15	-15.36	0.18	17.59	0.51	50.51
summer	Org	-0.19	-18.70	-0.03	-3.19	0.12	12.30
	Nitrate	-0.01	-1.50	0.04	4.48	0.10	10.48
	Sulfate	0.00	4.85	0.12	12.48	0.05	20.12
	Ammonium	0.02	1.59	0.07	7.01	0.12	12.40
	eBC(PM_1)	-0.02	-2.04	0.01	0.78	0.04	3.62
	HOA	-0.01	-0.76	0.00	-0.20	0.00	0.36
	BBOA	0.00	-0.47	0.01	0.77	0.02	2.01
	CCOA	-0.06	-5.37	-0.03	-2.74	0.00	0.27
	LO-OOA	0.00	0.02	0.03	3.26	0.07	6.54
	MO-OOA	-0.12	-11.80	-0.07	-6.62	-0.01	-1.44
	eBC(PM_{1HOA})	0.00	-0.03	0.00	-0.02	0.00	0.00
	eBC(PM_{1BBOA})	0.00	-0.26	0.00	0.36	0.01	0.99
	eBC(PM_{1CCOA})	-0.02	-2.18	-0.01	-1.04	0.00	0.11
	Tot PM_1	-0.24	-24.23	-0.07	-7.23	0.10	9.78
decade	Org	-0.09	-9.38	-0.03	-3.46	0.02	2.44
	Nitrate	-0.10	-10.35	-0.05	-5.02	0.00	0.32
	Sulfate	-0.04	-3.63	0.00	0.05	0.04	3.73
	Ammonium	-0.04	-3.85	-0.0.1	-0.77	0.02	2.33
	eBC(PM_1)	-0.08	-8.13	-0.05	-5.31	-0.03	-2.51
	HOA	-0.01	-0.52	0.00	-0.02	0.00	-0.25
	BBOA	-0.01	-0.95	0.00	-0.20	0.01	0.55
	CCOA	-0.03	-2.95	-0.01	-1.10	0.01	0.75
	LO-OOA	-0.03	-2.50	-0.02	-1.52	-0.01	-0.54
	MO-OOA	-0.03	-3.34	-0.01	-1.09	0.01	1.16
	eBC(PM_{1HOA})	0.00	-0.02	0.00	-0.02	0.00	-0.01
	eBC(PM_{1BBOA})	0.00	-0.49	0.00	0.26	0.00	-0.11
	eBC(PM_{1CCOA})	-0.01	-1.13	0.00	-0.42	0.00	0.29

Table S9: MK trends for "mass contribution" of all factors/chemicals in percentage for decades and seasons, based on the entire dataset, western and eastern air masses (% y^{-1}), detailed with lower confidence level (lcl), slope and upper confidence level (ucl).

Season	Chemicals	west			entire			east		
		lcl	slope	ucl	lcl	slope	ucl	lcl	slope	ucl
fall	Org	-1.61	-0.90	-0.19	0.30	0.35	0.41	-0.42	0.16	0.75
	Nitrate	0.13	0.32	0.51	0.02	0.19	0.37	-1.61	-0.90	-0.19
	Sulfate	-0.42	-0.31	-0.19	-0.36	-0.27	-0.18	-0.37	-0.03	0.32
	Ammonium	-0.15	-0.12	-0.09	-0.15	-0.13	-0.10	-0.38	-0.18	0.02
	eBC(PM_1)	-0.08	-0.06	-0.05	-0.05	-0.04	-0.03	-0.35	-0.20	0.02
	HOA	0.08	0.11	0.15	0.09	0.11	0.13	0.02	0.10	0.17
	BBOA	0.00	0.05	0.11	0.09	0.13	0.17	0.06	0.21	0.35
	CCOA	-0.04	0.01	0.06	-0.06	-0.02	0.02	-0.04	0.22	0.48
	LO-OOA	0.10	0.22	0.35	0.03	0.14	0.24	-0.72	-0.37	-0.03
	MO-OOA	-0.12	0.01	0.14	-0.17	-0.06	0.05	-0.63	0.22	0.20
	eBC(PM_{1HOA})	0.07	0.08	0.10	0.04	0.05	0.06	-0.03	-0.01	0.01
	eBC(PM_{1BBOA})	-0.14	0.05	0.23	0.21	0.35	0.48	-0.53	-0.13	0.26
	eBC(PM_{1CCOA})	-0.18	0.00	0.19	-0.45	-0.32	-0.19	-0.29	0.09	0.48
winter	Org	-0.93	-0.41	0.12	-0.22	-0.18	-0.15	-0.47	-0.16	0.15
	Nitrate	-0.29	-0.11	0.07	-0.03	0.13	0.28	-0.93	-0.41	0.12
	Sulfate	0.09	0.17	0.26	-0.07	-0.01	0.06	-0.05	0.16	0.36
	Ammonium	0.12	0.15	0.18	0.09	0.11	0.13	0.02	0.14	0.26
	eBC(PM_1)	-0.23	-0.21	-0.20	-0.20	-0.18	-0.17	0.02	0.16	0.23
	HOA	-0.14	-0.11	-0.09	-0.07	-0.05	-0.03	-0.07	-0.01	0.06
	BBOA	0.11	0.17	0.22	0.28	0.31	0.37	0.07	0.21	0.35
	CCOA	0.51	0.55	0.60	0.18	0.22	0.26	0.13	0.35	0.57
	LO-OOA	-1.01	-0.93	-0.85	-0.90	-0.84	-0.78	-0.86	-0.67	-0.47
	MO-OOA	0.10	0.20	0.29	0.18	0.26	0.34	-0.05	0.22	0.48
	eBC(PM_{1HOA})	-0.12	-0.11	-0.10	-0.07	-0.07	-0.06	-0.04	-0.03	-0.02
	eBC(PM_{1BBOA})	-0.84	-0.70	-0.55	0.03	0.13	0.24	-0.50	-0.25	0.00
	eBC(PM_{1CCOA})	0.71	0.85	1.00	-0.15	-0.05	0.05	0.05	0.29	0.54
spring	Org	-0.74	-0.24	0.26	0.12	0.17	0.23	-0.25	0.24	0.73
	Nitrate	-0.54	-0.34	-0.14	-0.53	-0.38	-0.22	-0.74	-0.24	0.26
	Sulfate	0.08	0.20	0.31	0.12	0.20	0.29	-0.17	0.11	0.39
	Ammonium	-0.07	-0.04	-0.01	-0.10	-0.08	-0.06	-0.18	-0.05	0.09
	eBC(PM_1)	-0.14	-0.13	-0.12	-0.14	-0.13	-0.12	-0.16	0.05	0.10
	HOA	-0.13	-0.11	-0.08	-0.03	-0.02	0.00	-0.05	0.00	0.05
	BBOA	-0.06	-0.03	0.01	-0.02	0.01	0.04	0.08	0.17	0.26
	CCOA	0.17	0.2	0.24	0.22	0.23	0.27	0.25	0.42	0.59
	LO-OOA	0.26	0.38	0.50	0.24	0.33	0.41	-0.34	-0.07	0.21
	MO-OOA	-0.65	-0.52	-0.40	-0.68	-0.59	-0.50	-0.79	-0.45	-011
	eBC(PM_{1HOA})	-0.14	-0.13	-0.12	-0.09	-0.08	0.07	-0.10	-0.09	-0.07
	eBC(PM_{1BBOA})	-0.95	-0.79	-0.63	-0.72	-0.62	-0.52	-0.64	-0.37	-0.10
	eBC(PM_{1CCOA})	0.74	0.89	1.05	0.57	0.66	0.76	0.19	0.45	0.72

Table S9 (continued)

Season	Chemicals	west			entire			east		
		lcl	slope	ucl	lcl	slope	ucl	lcl	slope	ucl
summer	Org	-0.20	0.13	0.44	-0.07	-0.01	0.05	-1.76	-1.17	-0.56
	Nitrate	-0.17	-0.06	0.05	-0.07	0.03	0.12	-0.2	0.13	0.44
	Sulfate	-0.12	0.01	0.14	-0.12	-0.01	0.09	-0.04	0.35	0.75
	Ammonium	-0.07	-0.04	-0.01	-0.03	-0.01	0.02	0.05	0.24	0.43
	eBC(PM_1)	-0.15	-0.14	-0.13	-0.10	-0.10	-0.09	0.07	0.21	0.38
	HOA	0.04	0.05	0.07	0.04	0.05	0.07	-0.05	0	0.05
	BBOA	0.02	0.04	0.07	0.05	0.07	0.09	0.04	0.12	0.20
	CCOA	0.02	0.05	0.08	-0.11	-0.09	-0.07	-0.40	-0.26	-0.12
	LO-OOA	0.33	0.44	0.55	0.49	0.58	0.67	0.46	0.79	1.12
	MO-OOA	-0.67	-0.57	-0.47	-0.71	-0.62	-0.53	-1.00	-0.63	-0.23
	eBC(PM_{1HOA})	-0.04	-0.03	-0.02	-0.02	-0.02	-0.01	-0.02	0.01	-0.03
	eBC(PM_{1BOA})	-0.11	0.04	0.18	0.49	0.60	0.72	1.12	1.48	1.83
	eBC(PM_{1CCOA})	-0.27	-0.13	0.01	-0.81	-0.70	-0.59	-1.91	-1.56	-1.22
decade	Org	-0.01	0.02	0.06	0.05	0.08	0.11	-0.14	0.09	0.33
	Nitrate	-0.11	-0.03	0.05	-0.13	-0.05	0.02	-0.58	-0.34	-0.10
	Sulfate	-0.01	0.04	0.10	-0.03	0.01	0.05	-0.09	0.05	0.20
	Ammonium	-0.01	0.01	0.02	-0.03	-0.02	-0.01	-0.08	0.00	0.07
	eBC(PM_1)	-0.17	-0.16	-0.16	-0.14	-0.13	-0.13	-0.13	-0.11	-0.09
	HOA	-0.04	-0.02	-0.01	0.00	0.01	0.02	-0.02	0.01	0.04
	BBOA	0.02	0.04	0.06	0.06	0.08	0.09	-0.02	0.03	0.08
	CCOA	0.17	0.19	0.21	0.05	0.07	0.08	-0.15	-0.05	0.04
	LO-OOA	-0.06	-0.01	0.05	0.04	0.08	0.12	-0.06	0.07	0.21
	MO-OOA	-0.23	-0.17	-0.12	-0.27	-0.23	-0.18	-0.17	-0.01	0.16
	eBC(PM_{1HOA})	-0.06	-0.06	-0.05	-0.04	-0.04	-0.03	-0.02	-0.01	0.00
	eBC(PM_{1BOA})	-0.41	-0.33	-0.25	0.02	0.08	0.14	0.05	0.20	0.35
	eBC(PM_{1CCOA})	0.31	0.38	0.46	-0.12	-0.06	-0.01	-0.37	-0.23	-0.08

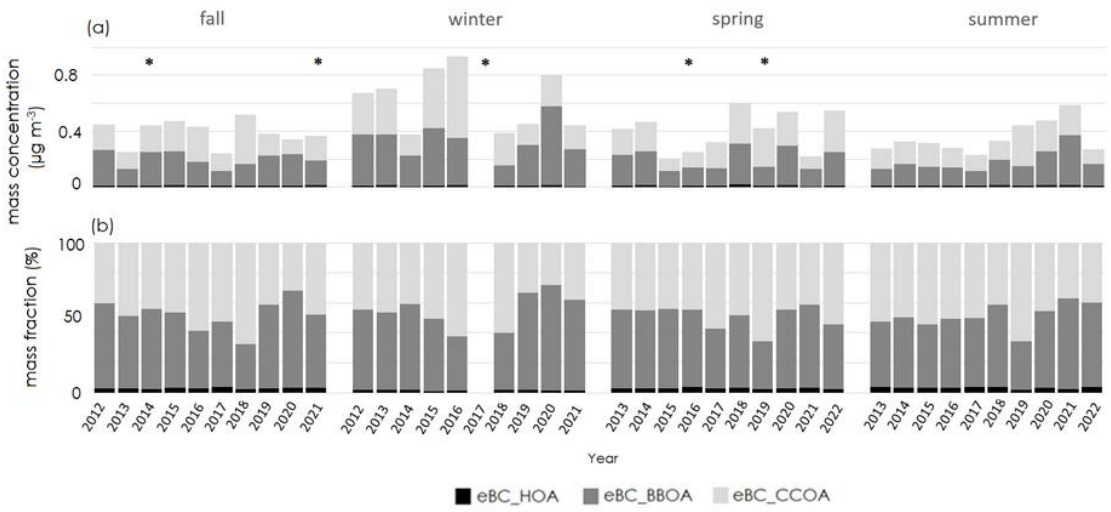

Fig. S6. (a) yearly mean mass concentration of the eBC contribution of POA, and (b) the corresponding mass contribution. Stars mean the data coverage is ≤ 1 month.

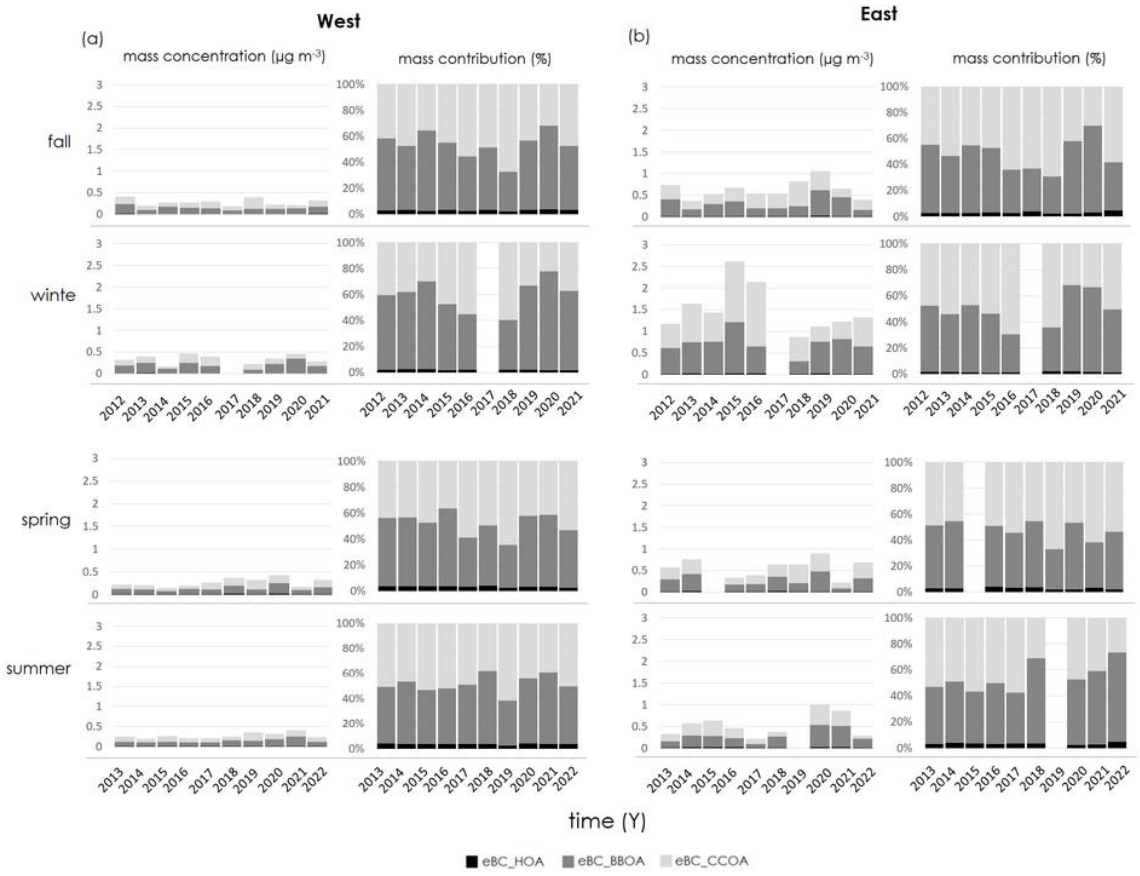

157

158 **Fig. S7. Yearly mean mass concentration and mass contribution of the eBC contribution of POA for (a) west and (b) east for different**
159 **meteorological seasons.**

160

161

162

163

164

165

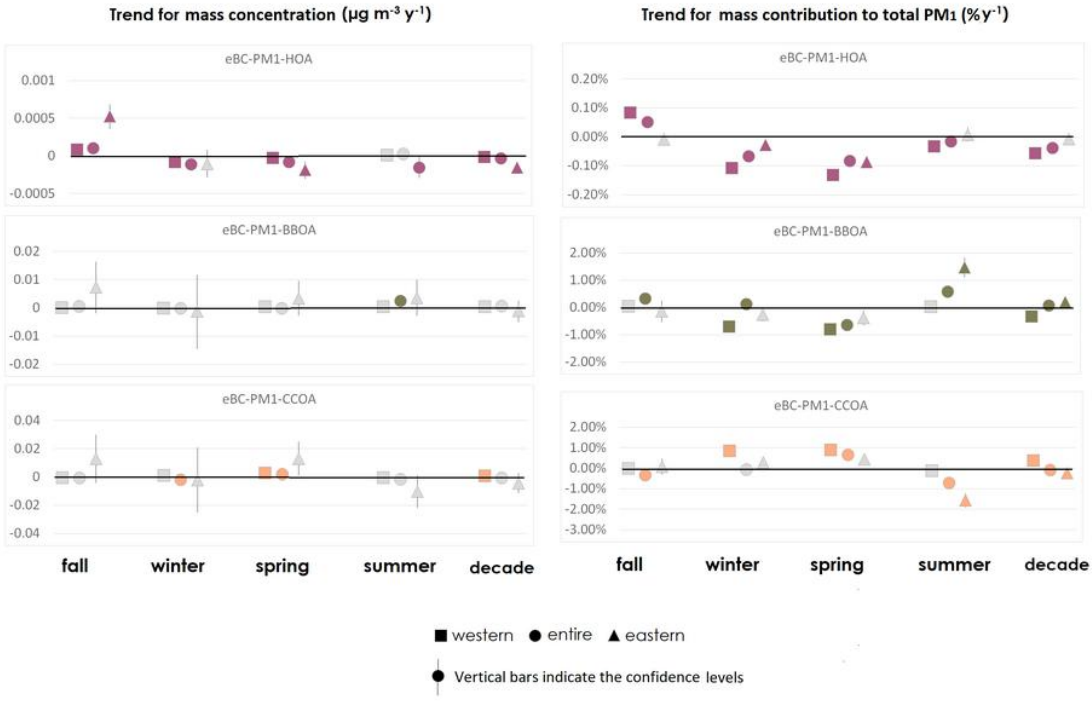

166

167 **Fig. S8. Seasonal MK trend results for Melpitz station with long time series based on different seasons and annual average for mass**
168 **concentration and mass contribution of POA factors on eBC-PM$_1$. The colored is statistically significant, whereas grey is not a**
169 **statistically significant trend. The slope of the western trend is shown by the square (■), entire by a circle (●), and eastern by a triangle**
170 **(▲), and vertical bars indicate the upper and lower confidence levels.**

171